Petrogenesis and Provenance of Ungrouped Achondrite Northwest Africa 7325 from Petrology, Trace Elements, Oxygen, Chromium and Titanium Isotopes, and Mid-IR Spectroscopy

[1,2]Cyrena A. Goodrich*

[3]Noriko T. Kita

[4]Qing-Zhu Yin

[4]Matthew E. Sanborn

[4]Curtis D. Williams

[3]Daisuke Nakashima**

[2]Melissa D. Lane

[1,5]Shannon Boyle

[1]Lunar and Planetary Institute, 3600 Bay Area Blvd, Houston, TX 77058 USA
goodrich@lpi.usra.edu

[2]Planetary Science Institute, 1700 E. Ft. Lowell Drive, Tucson, AZ 85719 USA

[3]WiscSIMS, University of Wisconsin-Madison, Madison, WI 53706 USA

[4]Department of Earth and Planetary Sciences, University of California at Davis, Davis, CA 95616 USA

[5]Department of Earth and Planetary Sciences, Rutgers University, Busch Campus, 610 Taylor Road, Piscataway, NJ 08854 USA

**Corresponding author*

***Present address: Tohoku University, Miyagi 980-8578, Japan.*

Submitted to Geochimica et Cosmochima Acta
May 2016

In press December 2016

Abstract

Northwest Africa (NWA) 7325 is an ungrouped achondrite that has recently been recognized as a sample of ancient differentiated crust from either Mercury or a previously unknown asteroid. In this work we augment data from previous investigations on petrography and mineral compositions, mid-IR spectroscopy, and oxygen isotope compositions of NWA 7325, and add constraints from Cr and Ti isotope compositions on the provenance of its parent body. In addition, we identify and discuss notable similarities between NWA 7325 and clasts of a rare xenolithic lithology found in polymict ureilites.

NWA 7325 has a medium grained, protogranular to poikilitic texture, and consists of 10-15 vol. % Mg-rich olivine (Fo 98), 25-30 vol. % diopside (Wo 45, Mg# 98), 55-60 vol. % Ca-rich plagioclase (An 90), and trace Cr-rich sulfide and Fe,Ni metal. We interpret this meteorite to be a cumulate that crystallized at ≥1200 °C and very low oxygen fugacity (similar to the most reduced ureilites) from a refractory, incompatible element-depleted melt. Modeling of trace elements in plagioclase suggests that this melt formed by fractional melting or multi-stage igneous evolution. A subsequent event (likely impact) resulted in plagioclase being substantially remelted, reacting with a small amount of pyroxene, and recrystallizing with a distinctive texture.

The bulk oxygen isotope composition of NWA 7325 plots in the range of ureilites on the CCAM line, and also on a mass-dependent fractionation line extended from acapulcoites. The ε^{54}Cr and ε^{50}Ti values of NWA 7325 exhibit deficits relative to terrestrial composition, as do ordinary chondrites and most achondrites. Its ε^{54}Cr value is distinct from that of any analyzed ureilite, but is not resolved from that of acapulcoites (as represented by Acapulco).

In terms of all these properties, NWA 7325 is unlike any known achondrite. However, a rare population of clasts found in polymict ureilites ("the magnesian anorthitic lithology") are strikingly similar to NWA 7325 in mineralogy and mineral compositions, oxygen isotope compositions, and internal textures in plagioclase. These clasts are probably xenolithic in polymict ureilites, and could be pieces of NWA 7325-like meteorites.

Using constraints from chromium, titanium and oxygen isotopes, we discuss two possible models for the provenance of the NWA 7325 parent body: 1) accretion in the inner solar system from a reservoir similar to that of acapulcoites in Δ^{17}O, ε^{54}Cr and ε^{50}Ti; or 2) early (< 1 Ma after CAI formation) accretion in the outer solar system (beyond the snow line), before ^{54}Cr and ^{50}Ti anomalies were introduced to this region of the solar system. The mid-IR emission spectrum of

NWA 7325 obtained in this work matches its modal mineralogy, and so can be compared with spectra of new meteorites or asteroids/planets to help identify similar materials and/or the parent body of NWA 7325.

1. INTRODUCTION

Northwest Africa (NWA) 7325 was found in Morocco in 2012 as 35 fresh-looking, dark green stones totaling 345 g in mass. It was reported to be an assemblage of Cr-Al diopside, calcic plagioclase, and forsterite with a "plutonic igneous" texture, and was classified as an ungrouped achondrite (Ruzicka et al., 2015). Since then, an additional five meteorites from northwest Africa have been found to be paired with NWA 7325, making a total mass >1.1 kg (Meteoritical Bulletin Database).

In initial work, Irving et al. (2013) described textures and mineral compositions of NWA 7325, and reported oxygen isotope compositions obtained for several subsamples by laser fluorination analysis. The oxygen isotope composition reported by Irving et al. (2013) fell within the broad compositional range shown by ureilites, and also on extensions from the established trends of acapulcoites and winonaites. Irving et al. (2013) also obtained bulk major and trace element compositions of cutting dust from NWA 7325 by XRF and ICP-MS. Based on the highly magnesian mineral compositions (low FeO content) and bulk Al/Si and Mg/Si ratios of NWA 7325 compared with data from the Messenger mission (Weider et al., 2012), Irving et al. (2013) suggested that this meteorite could be a plutonic rock excavated from Mercury.

However, the initial age dating of NWA 7325 yielded old ages of 4562.5±4.4 Ma from the Pb-Pb system (Amelin et al., 2013), and 4562.8±0.3 Ma from the ^{26}Al-^{26}Mg system (Dunlap et al., 2014). Based on these ages, Dunlap et al. (2014) argued that NWA 7325 was unlikely to be derived from the evolved crust of a planetary sized body, and that an origin on Mercury was therefore doubtful. These preliminary ages have now been refined (Koefoed et al., 2016) to a Pb-Pb age of 4563.4 ± 2.6 Ma and a ^{26}Al-^{26}Mg age of 4563.10±0.27 Ma relative to the D'Orbigny angrite anchor, indicating that NWA 7325 crystallized almost contemporaneously with the oldest achondrites such as the quenched angrites (e.g., D'Orbigny; Spivak-Birndorf et al., 2009; Schiller et al., 2010). Koefoed et al. (2016) concluded that the ancient age of NWA 7325 was an argument against formation of NWA 7325 on Mercury, but did not completely rule it out.

NWA 7325 has been investigated in many abstracts, and a significant amount of data for this meteorite is now available in three papers, including petrographic data, bulk chemical analyses, oxygen, carbon, nitrogen, strontium, xenon and argon isotope compositions, infrared and Raman spectra, and U-Pb and Al-Mg isotope systematics (Barrat et al., 2015; Koefoed et al., 2016;

Weber et al., 2016). These authors have all discussed the petrogenesis and origin of NWA 7325, and concluded that it is unlike any other known meteorite.

In this paper we investigate a new sample of NWA 7325. The results of our work augment data on petrography and mineral compositions, mid-IR spectroscopy, and oxygen isotope analyses given in previous publications, and add constraints from Cr and Ti isotope compositions on the provenance of the NWA 7325 parent body. In addition, we point out and discuss intriguing mineralogic and oxygen isotope similarities between NWA 7325 and clasts of a rare xenolithic lithology found in polymict ureilites (Ikeda et al., 2000; Kita et al., 2004).

2. SAMPLES AND METHODS

2.1. Optical and Electron Microscopy and Electron Microprobe Analyses (EMPA)

Two one inch round sections, one standard thin section and one thick section, were prepared from a 2.197 g sample of NWA 7325 that was purchased by our consortium. Both sections were first studied for petrography and mineral compositions. Optical and electron microscopy were performed in the Department of Geosciences at the University of Massachusetts (Amherst). Back-scattered electron images (BEI) was obtained using the Zeiss EVO50-XVP scanning electron microscope (SEM). Electron microprobe analysis (EMPA) and wavelength-dispersive (WDS) X-ray mapping were performed using the Cameca SX-50 electron microprobe. All analyses utilized natural and synthetic minerals, glasses, oxides and/or metals as standards. Silicate minerals were analyzed using 15 KeV and 30-60 nA beam current. Olivine grains were analyzed at 60 nA, with 100-400 second counting times for MnO, Cr_2O_3, Al_2O_3 and CaO, and 40 second counting times for MgO, FeO and SiO_2. Olivine cores in the Kenna ureilite were analyzed during every olivine probe run to ensure consistency with previous olivine data of Goodrich et al. (2013; and references therein) for ureilites and other olivine-rich achondrites. Plagioclase was analyzed at 10-20 nA with 5-20 second counting times and a slightly de-focused beam. Na_2O was always analyzed first to minimize loss during the analyses. Pyroxenes were analyzed at 30-40 nA with 10-30 second counting times. Sulfides and metal were analyzed using 15 KeV and 50 nA with 10-30 second counting times. Modal mineral abundances were obtained by point counting collages of BEI of the sections of NWA 7325.

Back-scattered electron imaging and EMPA of a magnesian anorthitic clast in polymict ureilite NWA 10657 (thin section #003) were obtained using the JEOL 8530-FE electron microprobe at ARES (Astromaterials Research and Exploration Science), Johnson Space Center. Analytical conditions were similar to those used at U. Mass.

2.2. Mid-Infrared Emission Spectroscopy

We also used mid-infrared emission spectroscopy to identify the mineralogy of NWA7325 through the use of a Fourier Transform infrared (FTIR) spectrometer. The emissivity technique uses radiation (heat) emitted from a sample to identify the mineralogy using diagnostic spectral features that deviate from ideal Planck blackbody radiation at a similar temperature. For this study, a Thermo Fisher Nicolet 6700 FTIR equipped with a CsI beamsplitter and an uncooled DTGS detector with a CsI window enabled spectral measurements to be acquired from 2000 to 230 cm^{-1} (i.e., 5-44 μm) at 2 cm^{-1} spectral sampling. This instrument is housed in the Vibrational Spectroscopy Laboratory at Stony Brook University and was modified for emission measurements by removing the instrument's internal Globar® (the IR source used for reflectance measurements) and allowing a heated sample in a glovebox exterior to the spectrometer housing to act as the infrared source, via a folding mirror that redirects the energy into the ray path of the spectrometer. The sample was heated to and maintained throughout measurement at approximately 70 °C and sat in a temperature-regulated environmental sample chamber within the external Plexiglas® glovebox. The system was purged with nitrogen to drive out other atmospheric gases (e.g., H_2O, CO_2) that otherwise would add spectral features to the data. The sample studied was the polished thick section of NWA 7325. The exposed surface of the meteorite on this section was roughly triangular with side lengths of ~12, 12, and 16 mm, allowing the ~1-cm diameter spot size of the instrument to investigate much of the cross-section of the meteorite chip.

Two blackbody target measurements (at ~70 and 100 °C) were obtained to determine the instrument response function and instrument temperature used for calibration. The emissivity spectra of the minerals were derived by reducing the raw wavelength- and temperature-dependent data by conversion of the sample's raw voltage data measured at the detector into calibrated sample radiance by dividing the voltage by the instrument response function, then dividing this sample radiance curve into the temperature-appropriate Planck blackbody curve.

The result is (unitless) sample emissivity that ranges from 0 to 1.0 (a blackbody would present an emissivity of 1.0 across the wavelength range).

2.3. Oxygen Isotope and Trace Element Analyses

Oxygen three-isotope analyses were performed by secondary ion mass spectrometry (SIMS) with the Cameca IMS 1280 at the University of Wisconsin (WiscSIMS) using a technique similar to that of Kita et al. (2010) and Goodrich et al. (2011). The Cs^+ primary ion beam was focused to ~15 μm with intensity of ~4nA. Secondary $^{16}O^-$ intensities were typically 4.5×10^9 cps and all three isotopes were detected using multicollection Faraday cups (FCs) with external reproducibility (spot-to-spot) of 0.3-0.4‰ for $\delta^{18}O$, $\delta^{17}O$ and $\Delta^{17}O$ ($=\delta^{17}O - 0.52 \times \delta^{18}O$). Several mineral standards (olivine, pyroxene, and plagioclase) were analyzed for calibration of instrumental biases as a function of the mineral compositions of unknowns (Supporting Information, Table S1), following the method in Tenner et al. (2013). We used the thick section of NWA 7325, which also included a San Carlos olivine standard for SIMS analyses. Eight sets of San Carlos olivine standard analyses bracket 7-12 unknown analyses to monitor instrumental bias.

Trace element analyses of plagioclase were performed after oxygen isotope analyses, similar to the method described in Kita et al. (2004). We used an O^- primary ion beam that is shaped to 15 μm diameter and intensity of ~3 nA. A total of 17 elements were analyzed by peak switching magnet field for ^{23}Na, ^{24}Mg, ^{27}Al, ^{28}Si, ^{39}K, ^{40}Ca, ^{45}Sc, ^{47}Ti, ^{52}Cr, ^{55}Mn, ^{57}Fe, ^{59}Co, ^{60}Ni, ^{63}Cu, ^{85}Rb, ^{88}Sr, and ^{138}Ba. The mass resolving power was set to ~5,000 (at 10% height) and no energy offset was applied. Contributions from molecular and hydride interferences to analyzed atomic ions are negligibly small. Single analyses took ~15 min. We used several plagioclase mineral and glass standards to estimate relative sensitivity factors (RSF) of trace element peaks to ^{28}Si (Supporting Information, Table S2), which are used to calculate the trace element concentrations. Detection limits for trace elements are typically lower than 30 ppb, except for Fe and Ni (~0.2 ppm). Direct ion imaging of analyzed spots were obtained for ^{23}Na, ^{24}Mg, ^{39}K, ^{40}Ca, and ^{52}Cr, after the trace element analyses to inspect micron-scale zoning of trace elements. The resolution of the ion image was ~2 μm.

199
200
201 **2.4. Chromium and Titanium Isotope Analyses**
202 Analyses of the Cr and Ti isotopic compositions of a bulk sample of NWA 7325 were made
203 using a 20.94 mg aliquot of homogenized sample powder. A separate 30.31 mg sample of the
204 acapulcoite type specimen, Acapulco, was also prepared. The samples were dissolved by placing
205 the powders into a PTFE Parr digestion capsules along with a 2:1 mixture of ultraclean
206 concentrated HF-HNO_3. The PTFE capsules were placed into stainless steel jackets and heated
207 in a 190 °C oven for 96 hours. After digestion in the oven, the samples were treated by re-
208 dissolving the samples in alternating solutions of 6 N HCl and concentrated HNO_3 to eliminate
209 fluorides formed during the dissolution process. The Cr was isolated from the bulk matrix of
210 each sample using a 3-column chromatography procedure previously described by Yamakawa et
211 al. (2009).
212 Chromium isotopic measurements were made using the Thermo *Triton Plus* thermal
213 ionization mass spectrometer (TIMS) at the University of California at Davis (UC Davis). The
214 Cr was loaded onto previously outgassed W filaments by mixing 3 μg of Cr with an Al-silica
215 gel-boric acid activator with a total load of 12 μg (four filaments in total). The sample filaments
216 were bracketed by two terrestrial standard filaments before and after loaded with 3 μg of NIST
217 SRM 979 on each filament. Each filament analysis consisted of 1200 ratios (48 block of 25
218 ratios) with an 8 second integration time. The intensity of ^{52}Cr was set to 10 V (±15%) with a
219 gain calibration completed at the start of each filament and a 60 second baseline measured at the
220 start of each block. The Faraday cup amplifiers were rotated after every block to eliminate any
221 issues due to variations in cup efficiencies. Instrumental mass fraction of the Cr isotope ratios
222 was corrected using an exponential law and a $^{50}Cr/^{52}Cr$ ratio of 0.051859 (Shields et al., 1966).
223 Titanium was separated from the remaining matrix using a combination of cation and anion
224 exchange chromatography following the methods of Zhang et al. (2011). Titanium yields after
225 processing through both cation and anion chromatography were greater than 98%. Titanium
226 isotope ratios were measured with a Thermo *Neptune Plus* multi-collector inductively coupled
227 plasma mass spectrometer (MC-ICP-MS) at UC Davis. A standard H-type skimmer cone was
228 used, while a Jet sample cone was inserted in place of the standard sample cone. Typical
229 intensity for ^{48}Ti was 25V (10^{11}ohm resistors) for a 1 ppm solution run in high-resolution mode

(MSRP ~8000). The isotope ratios were measured in multi-dynamic mode on Faraday cups in two peak jumping steps, measuring $^{44}Ca^{+}$, $^{46}Ti^{+}$, $^{47}Ti^{+}$, $^{48}Ti^{+}$, $^{49}Ti^{+}$, $^{50}Ti^{+}$ (in step 1) and $^{49}Ti^{+}$, $^{51}V^{+}$, $^{53}Cr^{+}$ (in step 2). The external reproducibilities (2SD) for internally normalized (to a $^{49}Ti/^{47}Ti$ ratio of 0.749766 [Niederer et al., 1985]) $\varepsilon^{46}Ti$, $\varepsilon^{48}Ti$, and $\varepsilon^{50}Ti$, based on repeated analyses of pure SPEX Ti solution, are 0.48, 0.23, and 0.53, respectively, consistent with theoretical expectations.

3. RESULTS

3.1. Petrography and Mineral Compositions

Both sections show a protogranular to poikilitic texture of high-Ca pyroxene (~0.25–1 mm) and olivine (~0.1-0.7 mm) grains, surrounded or poikilitically enclosed by plagioclase (Fig. 1). Olivine grains are rounded and commonly occur as partial or complete mantles around pyroxenes (Fig. 1, 2a). Modal abundances for the two sections are (by area) ~25-30% pyroxene, 10-15% olivine and 55-60% plagioclase, with trace amounts of sulfide and metal. These values are similar to modal abundances reported by Irving et al. (2013) and Barrat et al. (2015), but differ from those (2% olivine and 44% pyroxene) reported by Weber et al. (2016). The sections also contain several area % voids with shapes similar to those of the olivine (Fig. 1). The voids may represent former (plucked) olivine grains, but are not included in the modal abundances.

Olivine and large pyroxene grains are homogeneous with compositions of Fo 97.5±0.1, and Wo 45.3±0.2, Mg# 98.2±0.2, respectively (Table 1, Figure 3,4,5). Major and minor element compositions are consistent with those of Barrat et al. (2015) and Weber et al. (2016). The large pyroxene grains show polysynthetic twin lamellae in crossed polarized light and BEI (S4).

As noted by Irving et al. (2013) and Weber et al. (2016), plagioclase has a mottled appearance (Figs. 2b-d). Near contacts with olivine or pyroxene it contains patches of tiny Ca-rich pyroxene (identity inferred from BEI, x-ray maps, and mixed EMP analyses) and sulfide grains (Fig. 2b,c,d,f). These inclusions sometimes show elongated shapes and parallel alignment, suggesting crystallographic control by the plagioclase. Olivine grains have smooth edges along contacts with plagioclase (Fig. 2d). In contrast, pyroxene grains show resorbed edges along contacts with plagioclase, with numerous idiomorphic re-entrants of plagioclase (Fig. 2b,c). Plagioclase also commonly intrudes into pyroxene grains as veins with idiomorphic side protrusions (Fig. 6a).

EMPA profiles in the plagioclase, beginning at contacts with pyroxene or olivine and extending into the interiors of plagioclase grains show that analyses near the contacts have excesses of CaO (leading to artificially high An content), MgO (up to ~6 wt.%), and FeO (up to ~0.5 wt.%), as well as deficits of Si+Al, relative to the "cleaner" analyses from the interior, as a result of overlap with the small pyroxene inclusions in the analyses (see S5). Based on these observations, we defined "clean" plagioclase analyses as those having MgO <0.5 wt.%, SO_2 below detection limit (0.04 wt. %) and molar Si+Al (calculated on the basis of 8 oxygen atoms) of 3.97-4.02. A compilation of 166 "clean" analyses (Table 1; Fig. 5) showed an average composition of An 89.7±1.2, with 0.03±0.02 wt.% FeO and 0.3±0.1 wt.% MgO. K_2O contents were below detection limit of 0.04 wt. % in all analyses. This composition is consistent with an average of 71 plagioclase analyses given by Barrat et al. (2015), although these authors do not report whether their data were selective. In contrast, Weber et al. (2016), reported six "representative" plagioclase analyses with a wider range of An (79.3-93.5) and higher FeO and MgO contents. The compositions of Weber et al. (2016) are within the range of all plagioclase compositions we measured and, by comparison to our observations, may have been contaminated by tiny pyroxene inclusions.

Furthermore, we found that even the "clean" interior areas of plagioclase in NWA 7325 are not homogeneous (Fig. 6), but are pervaded by fine linear features (≤2 μm wide). In BEI, these appear as darker zones (lower average Z than surrounding plagioclase) with central areas consisting of "rosettes" or equigranular crystals (Fig. 6c) of a brighter phase (higher average Z than surrounding plagioclase). Based on x-ray maps (Figs. 6d-f), the high-Z phase has higher Al and Mg and much lower Si contents than the surrounding plagioclase, while the darker zones are similar to the plagioclase but more sodic. From these observations we infer that the veins consist of Na-enriched plagioclase plus crystals of Mg-Al spinel. SIMS ion images are consistent with this interpretation (see section 3.4 and S6).

The plagioclase also contains small (~10 to 150 μm diameter) "islands" of pyroxene that show reaction with the plagioclase (Fig. 7). Elemental x-ray maps show that plagioclase immediately surrounding and intruding into these pyroxene grains is enriched in Na relative to the average plagioclase composition (Fig. 7a,b). Many of these grains show zonation in BEI, with darker cores and brighter rims (Fig. 7c; S4). EMPA profiles across such grains show that the rims are enriched in Ca and Fe, and depleted in Mg, Al and Na. relative to the cores (e.g.,

292 Fig. 7d). Furthermore, some of these grains (e.g., Fig. 7c) have outer rims of dendritic crystals
293 that appear to be wollastonite, based on x-ray maps and broad beam analyses.
294 Sulfides occur as patches of tiny grains dispersed within plagioclase (Fig. 2b,c). In some
295 places along plagioclase-boundaries, there are patches of sulfide that appear to have been melted
296 and dispersed among re-crystallized plagioclase laths (Fig. 2f). In addition, sulfides occur as
297 ~10-60 μm-sized grains, with rounded to irregular shapes, included in any of the silicates or
298 along grain boundaries (Fig. 2e). Some contain small blebs of Fe,Ni metal. They commonly
299 show thin lamellae of a Cr-enriched sulfide (Fig. 2e). These lamellae are too small to analyze,
300 but are likely daubréelite. The sulfides are troilite with ~3.9 wt.% Cr and ~0.3 wt.% Ni (average
301 of 13 analyses avoiding Cr-rich lamellae). None of the metal grains were large enough to
302 analyze cleanly, but minimum values of ~8 to 15 wt.% Ni and ~2.5 to 5.6 wt.% Co are given by
303 analyses that overlapped silicates.
304
305 **3.2. Mid-IR Emission Spectra**
306 An average of 9 emissivity spectra of the polished thick section is shown in Fig. 8. This
307 spectrum exhibits deep fundamental bands because the polished surface eliminates any volume
308 scattering features in the spectrum. Using a spectral library of 52 different rock-forming
309 minerals (Table 2), including a range of feldspar, pyroxene, and olivine compositions, and other
310 mineral classes, the meteorite spectrum was spectrally unmixed over the spectral range of 2000
311 to 300 cm^{-1}, according to the linear-retrieval algorithm (linear least squares) of Ramsey and
312 Christensen (1998), in order to determine the mineralogic composition of the meteorite chip.
313 The model fit to the laboratory spectrum indicates that the meteorite sample consists of 57 vol. %
314 anorthite (An_{89}), 32.8 vol. % diopside (Fs_1Wo_{49}), and 10.2 vol. % forsterite (Fo_{100}) (Fig. 8).
315 Although pyrite and troilite were in the spectral endmember library, no Fe sulfide was identified
316 through mathematical unmixing of the meteorite spectrum, likely because troilite is present in
317 only trace amounts in the meteorite.
318 These spectral unmixing results coincide well with the mineral compositions and modal
319 abundances determined from petrographic studies and EMPA in this work and in other
320 petrologic studies (Irving et al., 2013; Barrat et al., 2015), but vary from results by Weber et al.
321 (2016) who studied a thin section of NWA 7325 that contains much less olivine (2 vol.%) and
322 more pyroxene (44%) than our sections. The polished-thin-section reflectance spectrum of

Weber et al. (2016) (acquired over an area of 4 x 4 mm and shown in their Figure 6b) was converted to an emissivity spectrum via Kirchhoff's Law (where emissivity = 1 – reflectivity). The converted Weber et al. spectrum is shown at the bottom of Figure 8 superposed on our meteorite emissivity spectrum of the polished thick section. The spectral shapes for the two meteorite spectra are similar, with the largest difference being the pronounced band at 1105 cm^{-1} (~9 μm) in the Weber et al. (2016) thin section data that likely is due to the higher abundance of diopside in their section compared with the sections we studied.

3.3. Oxygen Isotopes

We obtained a total of 19 analyses of NWA 7325 from olivine, pyroxene and plagioclase (Supporting Information, Table S3). As shown in Fig. 9a, these data plot on the CCAM (Carbonaceous Chondrite Anhydrous Mineral) line within the region of bulk ureilite data (Clayton et al., 1977; Clayton and Mayeda, 1996, 1999). Except for one deviant analysis in plagioclase, $\delta^{18}O$ and $\delta^{17}O$ values of individual mineral phases are homogeneous within analytical uncertainties. We intentionally aimed at both the core and the rim of a zoned pyroxene crystal (similar to Fig. 7c; S4), and found that they do not show any significant difference (Table S3). The one analysis of plagioclase that is deviant overlapped with a dark vein (similar to those in Fig. 6). This analysis showed slightly higher $\delta^{18}O$ and $\delta^{17}O$ values by 0.7 ‰, and higher $\Delta^{17}O$ by 0.3‰ (Table S3), compared with the rest of analyses. If this analysis was a mixture between clean plagioclase and the darker vein, then the vein could have much higher $\delta^{18}O$, $\delta^{17}O$ and $\Delta^{17}O$ values. Shock melting, which we infer to have produced these dark veins (see below), should not have produced a change in $\Delta^{17}O$. The deviant composition of the veins could, however, result from preferential weathering of such veins in the terrestrial desert environment.

Excluding this analysis, the average values in each mineral are shown in Table 3. The $\delta^{18}O$ values of the three minerals increase slightly from pyroxene (7.3 ‰), to olivine (7.6‰) to plagioclase (7.9‰), with indistinguishable $\Delta^{17}O$ values. Using the modal abundances of the three minerals, we estimate the bulk oxygen isotope composition of NWA 7253 to be $\delta^{18}O$ = 7.7±0.4‰, $\delta^{17}O$ = 3.1±0.3‰ (Table 3). The average of 18 spot analyses gives $\Delta^{17}O$= – 0.90±0.13‰. Figure 9a also shows oxygen isotope compositions determined from bulk samples of NWA 7325 by Irving et al. (2013), Barrat et al. (2015) and Weber et al. (2016). The bulk

sample analyses show some variation within the range of all the SIMS analyses. In addition, Jabeen et al. (2014) reported oxygen three isotope ratios of plagioclase and pyroxene separates from NWA 7325 obtained by CO_2 laser fluorination mass spectrometer analyses. The SIMS plagioclase data match very well with their plagioclase separates, while the SIMS pyroxene data are ~ 1‰ higher in $\delta^{18}O$ than their pyroxene separate. The reason for the discrepancy is not clear.

3.4. Trace Elements in Plagioclase

We obtained nine trace element analyses from four plagioclase grains that were also analyzed for oxygen isotopes. Among them, seven analyses were made on clean plagioclase and two analyses were on a dark zoned vein. Individual spot data are given in Supporting Information, Table S2. Concentrations of Ni are near the detection limit (0.2 ppm). The average and 1SD of seven clean analyses are shown in Table 4 and Figure 10 for selected elements. Most trace element data show some variability (10-30% in SD) and some analyses show correlated increases in Mg, Sc, Ti, Cr, Mn, and Fe (Table S2). The enrichment of these elements could be related to the presence of small pyroxene crystals in the plagioclase (as described above). MgO and FeO contents of clean plagioclase are calculated to be 0.235% and 0.052%, respectively, consistent with electron microprobe analyses (Table 1).

Analyses on dark zoned veins showed 10-20% lower ^{28}Si signals and higher Al, consistent with the inference from electron microprobe analyses that these areas contain μm-sized spinel grains (above). Ion images taken after the analyses show μm-sized inclusions rich in Mg and Cr (S6), consistent with the electron probe observations (Fig. 6).

3.5. Chromium and Titanium Isotopes

Chromium and Ti isotopic compositions were obtained in powdered, bulk samples of NWA 7325 and Acapulco (acapulcoite). Deviations of the internally normalized stable $^{54}Cr/^{52}Cr$ and $^{50}Ti/^{47}Ti$ isotope ratios from the terrestrial isotopic composition are presented in Table 5 and Figure 11. The Cr isotope ratios of both NWA 7325 and Acapulco exhibit deficits relative to the terrestrial composition with an $\varepsilon^{54}Cr$ of -0.61 ± 0.11 and -0.70 ± 0.10, respectively. Deficits in the ^{50}Ti isotope are also observed in NWA 7325 and Acapulco with $\varepsilon^{50}Ti$ of -1.51 ± 0.53 and -1.31 ± 0.27, respectively, whereas ^{46}Ti and ^{48}Ti are unresolved from terrestrial composition.

4. DISCUSSION

4.1. Mineralogy and Mineral Compositions of NWA 7325 Compared With Those of Other Achondritic Materials

As discussed by Weber et al. (2016), olivine in NWA 7325 is similar to olivine in some winonaites and acapulcoites/lodranites in its very high Fo content. However, compared with any known achondrite, its Fe/Mg-Fe/Mn composition is unique, and notable for showing subchondritic Mn/Mg (Fig. 3a). Its CaO-Cr_2O_3 composition is also unique, with Cr_2O_3 significantly higher than in any olivine-rich achondrites except ureilites, and CaO higher than in ureilites of similar Cr_2O_3 content (Fig. 3b). Likewise, pyroxene in NWA 7325 is similar to pyroxenes in some winonaites and acapulcoite/lodranites in Mg# and Wo, but differs in having higher Al_2O_3 (Fig. 4). Plagioclase in NWA 7325 is similar to plagioclase in angrites (Keil, 2012) in its very high An contents (Fig. 5), but has much lower FeO (Fig. 5, 10). It is distinguished from plagioclase in any other achondrites (Mittlefehldt et al., 1998; Krot et al., 2013) by higher An, as well as higher MgO (Fig. 5, 10a). Overall, the combination of very calcic plagioclase and very magnesian mafic silicates in NWA 7325 is not observed in any other achondrite (Fig. 5). This is further evidenced by the mid-IR emission spectra of the NWA 7325 (Fig. 8), which accurately reflects its mineralogy but does not match the spectrum of any studied meteorite (e.g., Ashley, 2011). Thus, we conclude that NWA 7325 does not belong to any known meteorite group, in agreement with Barrat et al. (2015) and Weber et al. (2016).

There is, however, another source of achondritic material with which NWA 7325 can be compared – i.e., achondritic lithologies that have been found only as clasts in meteorite breccias. Polymict ureilites, for example, contain a significant component of feldspathic clasts (Prinz et al., 1988; Ikeda et al., 2000; Cohen et al., 2004; Kita et al., 2004; Goodrich and Wilson, 2014). The majority of these clasts appear to represent two distinct lithologies, the "albitic lithology" and the "labradoritic lithology", which have been interpreted as indigenous to the ureilite parent body based on oxygen isotopes and argued to represent crustal rocks complementary to the residual ureilites (Ikeda et al., 2000; Cohen et al., 2004; Goodrich et al., 2004; Kita et al., 2004; Bischoff et al., 2014).

Although the plagioclase in the albitic (An 0-32) and labradoritic (An 33-69) lithologies is more sodic than plagioclase in NWA 7325 (Fig. 5), polymict ureilites also contain a less

abundant population of feldspathic clasts that consist of very calcic plagioclase and very magnesian olivine and/or pyroxene, strikingly similar to the characteristic assemblage of NWA 7325 (Fig. 5). Literature data are available for five of these clasts (Ikeda et al., 2000; Cohen et al., 2004; Kita et al., 2004), of which one (clast γ-8 in polymict ureilite DaG 319; Ikeda et al., 2000 and Kita et al., 2004) consists of plagioclase and olivine, two consist of plagioclase and pyroxene, and two consist only of plagioclase. In addition, we found and analyzed a new magnesian anorthitic clast in polymict ureilite NWA 10657. The sizes of these clasts (mostly at the low end of the range 10-500 μm) compared with grain sizes in NWA 7325 would be consistent with unrepresentative sampling of their complete mineral assemblages.

All six of these clasts have plagioclase compositions in the range An 86-96, similar to NWA 7325 (Fig. 5). Olivine in clast γ-8 has Fo (93), Fe/Mn ratio, and CaO and Cr_2O_3 contents similar to olivine in NWA 7325 (Fig. 3,5). Pyroxene in the pyroxene-bearing clasts have Wo (45-48), Mg# (95-98), and Al_2O_3 contents similar to pyroxene in NWA 7325 (Table 1; Fig. 4). Iron contents in plagioclase in four of these clasts are very low (<0.03 wt.% FeO), similar to NWA 7325. Moreover, two of these clasts show internal textures in plagioclase that strongly resemble the internal textures of plagioclase in NWA 7325 (Fig. 12; cf. Figs 6 and 7), including small, dispersed pyroxene grains, reacted "islands" of high-Ca pyroxene, and "veins" of Na-enriched plagioclase + (apparently) spinel. Notably, these two clasts both show high FeO contents in plagioclase (~0.5 wt %), even in areas that apper to be free of inclusions in BEI, similar to plagioclase in NWA 7325.

Oxygen isotope compositions have been determined for two of these clasts (Kita et al., 2004) and plot on the CCAM line, very similar to the bulk composition of NWA 7325, within the range of ureilites (Fig. 9b). Despite the ureilite-like oxygen isotope composition of this lithology in polymict ureilites, it is unlikely to be indigenous to the ureilite parent body because petrologic modeling indicates that plagioclase this calcic could not have been produced on the ureilite parent body (Kita et al., 2004; Goodrich et al., 2016a). Therefore, these clasts are probably xenolithic, and could represent fragments of the NWA 7325 parent body. This is plausible, because polymict ureilites are known to contain a large variety of chondritic and achondritic xenoliths (Prinz et al., 1986, 1987a,b; Ikeda et al., 2000; Goodrich et al., 2004, 2016b; Kita et al., 2004; Downes et al., 2008; Horstmann and Bischoff , 2014).

447 **4.2. Equilibration Temperatures for NWA 7325**

448 Based on the distribution of Ca between olivine and high-Ca pyroxene (Köhler and Brey,
449 1990), the calculated equilibration temperature for NWA 7325 (using the large, unzoned
450 pyroxene grains) is 1180°C. This is similar to Ca distribution temperatures for ureilites and a
451 few brachinites, but higher than those of most other olivine-rich achondrites (e.g., Day et al.,
452 2012; Gardner-Vandy et al., 2013; Goodrich et al., 2015).

453 The distribution of oxygen isotopes between minerals can also provide an estimate of
454 equilibration temperatures. The oxygen isotope fractionations between minerals in NWA 7325
455 obtained from SIMS analyses are small (less than 1‰), which suggests formation of these
456 minerals at igneous temperatures. In contrast, Jabeen et al. (2014) reported 1.6‰ fractionation
457 between $\delta^{18}O$ values of diopside and plagioclase, from which they argue that oxygen isotopes in
458 NWA 7325 show characteristics of large planetary sized bodies, like Earth and Mars. A
459 fractionation of 1.6‰ in $\delta^{18}O$ between diopside and An_{90} translates to an equilibrium
460 temperature of ~400 °C (Clayton and Kieffer, 1991), which is unreasonably low given the
461 petrologic characteristics of NWA 7325. An absence of large mass-dependent fractionation of
462 oxygen isotopes is characteristic of high-temperature igneous differentiation under dry
463 conditions, such as those among lunar samples (e.g., Spicuzza et al., 2007), but not an indicator
464 of sizes of planetary bodies.

465

466 **4.3. Petrogenesis of NWA 7325**

467 The subchondritic Mn/Mg ratio of olivine of NWA 7325 (Fig. 3a) indicates that this
468 meteorite is either a residue of a high degree of partial melting or a cumulate formed at high
469 degrees of fractional crystallization of a melt (Goodrich and Delaney, 2000). Its high abundance
470 of plagioclase, which suggest a basaltic composition, as well as its poikilitic texture, suggest that
471 a cumulate origin is more likely, as interpreted by Irving et al. (2013) and Weber et al. (2016).
472 In addition, Barrat et al. (2015) discussed constraints from bulk REE abundances that provide
473 strong support for a cumulate, rather than residue, origin.

474 Thus, NWA 7325 is a "crustal" rock, a product of a partial melt generated on its parent
475 asteroid. In contrast, the majority of primitive achondrites (e.g., ureilites, brachinites,
476 acapulcoites and lodranites, winonaites) are olivine-rich, plagioclase-depleted rocks thought to
477 be asteroidal residues (Krot et al., 2013). The few known plagioclase-rich achondrites thought to

be crustal samples, e.g., GRA 06128/06129 (Shearer et al., 2010; Day et al., 2012), NWA 6704/6693/6926 (Irving et al., 2011; Warren et al., 2013) and NWA 8186 (Srinivasan et al., 2015), as well as the most abundant types of feldspathic clasts in polymict ureilites, all have significantly more sodic plagioclase than NWA 7325 (Fig. 5). Thus, not only does NWA 7325 not belong to any known primitive achondrite group, it cannot be related any known group as a complementary crustal sample. Thus, there is no known meteorite that can provide an exact analogy for the petrogenesis of NWA 7325.

NWA 7325 appears to have crystallized from a generally basaltic melt that was depleted in incompatible elements (see next section), under conditions of very low oxygen fugacity (~IW-2.9, similar to the most reduced ureilites; Sutton et al., 2016). Pyroxene and olivine were the earliest phases to crystallize from this melt at temperatures ≥1180 °C, with plagioclase growing later around them. The abundance of plagioclase in NWA 7325 (~60%) is too high for the rock to represent a melt composition (cf. the Ol-Plag-Qtz phase system for Mg-rich systems; Longhi, 1991), so it is mostly likely a cumulate. Its texture (except features resulting from secondary processes discussed below) is similar to that of heteradcumulates in terrestrial layered igneous complexes, in which poikilitic crystals (in this case, plagioclase) grow from pore liquids surrounding cumulus crystals (Wager and Brown, 1967; Hunter, 1996). Considering its probable asteroidal (rather than planetary) origin, it likely formed in a subvolcanic environment.

4.3.1. Secondary petrologic processes

At some time after primary crystallization of NWA 7325, plagioclase and sulfides (the phases with the lowest melting temperatures) were remelted and the melt reacted with small pyroxene grains that had been included in the plagioclase. The small, zoned pyroxene grains now observed in plagioclase (Fig. 7, S4) suggest the reaction:

$$\text{plagioclase } (An_{90}Ab_{10}) + \text{diopside} = \text{wollastonite} + \text{albite} \quad (1).$$

The pervasive mottled veins in plagioclase (e.g., Fig. 4) suggest the reaction:

$$\text{plagioclase } (An_{90}Ab_{10}) + \text{diopside} = \text{spinel} + \text{albite} \quad (2).$$

However, neither of these proposed reactions can be balanced. In equation [1], Mg is not accounted for in the products. In equation [2], Ca is not accounted for in the products. This suggests that the overall reaction that occurred (neglecting the sulfides, which would have melted and re-crystallized without reaction with silicates) was:

509 plagioclase ($An_{90}Ab_{10}$) + diopside-rich pyroxene =

510 Wo-enriched pyroxene + Mg-rich spinel + Na-enriched plagioclase (3).

511 This total reaction requires significant mobility of cations and therefore implies a high degree of
512 melting of the plagioclase, possibly total melting.

513 Based on the presence of mechanical twinning in the pyroxenes (a common effect of shock;
514 Stöffler et al., 1991), and by analogy to enstatite chondrite impact melt rocks that have some of
515 the same textural features observed in NWA 7325 plagioclase (Keil, 2007), we suggest that this
516 remelting of plagioclase and sulfides was caused by impact-related shock. In contrast, Bischoff
517 et al. (2013) and Weber et al. (2016) argued that it was due to internal reheating, possibly by a
518 nearby dike-like intrusion (contact metamorphism), followed by rapid cooling. Their arguments
519 against a shock origin include the paucity of standard shock features in olivine and the absence
520 of significant Ar loss. However, selective shock melting of low melting-temperature phases can
521 occur at relatively low degrees of shock (e.g., Warren and Rubin, 2010). Furthermore, it is not
522 clear what could have caused rapid cooling of a subvolcanic cumulate rock other than excavation
523 by an impact event. Rapid total melting and only limited reaction with other phases (e.g., small
524 pyroxene inclusions), such as would occur in a shock event, is also supported by the lack of
525 evidence for disturbance of the ^{26}Al-^{26}Mg isochron for NWA 7325 (Dunlap et al., 2014; Koefoed
526 et al., 2016).

527 An important question, given the extremely low FeO contents of "clean" plagioclase areas in
528 NWA 7325 (potentially a signature feature for NWA 7325-like material) is how FeO might have
529 been re-distributed during this reaction. One possibility is that FeO from the melted plagioclase
530 was preferentially partitioned into the newly crystallizing spinel and Wo-rich pyroxene. In this
531 case, the FeO contents of clean plagioclase in NWA 7325 must be lower than they were in the
532 primary plagioclase in these rocks. This would suggest that plagioclase in NWA 7325-like
533 materials that did not experience this re-melting could have higher FeO contents, while only the
534 "clean" plagioclase in remelted areas has such low FeO. However, this suggestion is not
535 supported by observations of the clasts of the magnesian anorthitic lithology in polymict ureilites
536 that have been studied so far, assuming that these clasts represent NWA 7325-like material. The
537 four clasts that have very low FeO contents in plagioclase were not reported to have textures like
538 those in NWA 7325 plagioclase (Ikeda et al., 2000; Cohen et al., 2004; Kita et al., 2004),
539 whereas the two clasts that show internal plagioclase textures like those in NWA 7325 (Fig. 12),

showed much higher FeO contents, even in apparently "clean" (inclusion-free) areas. This suggests the possibility that even these areas are not pure plagioclase, but instead have inclusions of mafic phases (such as pyroxene and spinel) on a scale much smaller than a micron. Additional investigations into these textures in NWA 7325 and the magnesian anorthitic clasts in polymict ureilites could therefore be critical for future attempts to recognize NWA 7325-like materials among meteoritic materials.

4.4. Trace Elements in the Parental Melt of NWA 7325

Concentrations of Mg, Fe, K, Sr, Ti, and Ba in seven analyses of clean plagioclase are compared in Fig. 10 with those of plagioclase in several other types of achondrites. Plagioclase in NWA 7325 is highly depleted in Fe, K, Ti, and Ba compared with plagioclase in eucrites, angrites and the ungrouped basaltic achondrite NWA 011 (Hsu and Crozaz, 1996, 1997; Floss et al., 2003, 2005). Low Fe contents are obviously related to the high Mg# of NWA 7325 compared with other achondrites. Lower Ti and Ba concentrations in plagioclase in NWA 7325 distinguish it from those in other achondrites. Although partition coefficients for some of these elements between plagioclase and melt decrease with anorthite contents (Bindemann et al., 1998; Dohmen and Blundy, 2014), most of the plagioclase shown in Fig. 10 (i.e., angritic and eucritic) is also anorthite-rich, similar to that of NWA 7325. Thus, the NWA 7325 parental melt must have been significantly depleted in incompatible element abundances compared with those in other anorthite-bearing achondrites. Barrat et al. (2015) reported bulk trace element abundances of NWA 7325, showing depletion in alkali elements (Na, K, Rb) and incompatible trace elements (REEs), but a high positive Eu anomaly. Our SIMS trace element analyses of plagioclase are generally consistent with the bulk data, e.g., the high Sr concentrations in plagioclase are consistent with the Eu anomaly being caused by strong partitioning of Eu^{2+} into plagioclase at low oxygen fugacity. However, in contrast to the high bulk Ba concentrations reported in Barrat et al. (2015) ,which were interpreted to be due to terrestrial weathering in a hot desert environment, we found depleted Ba concentrations in plagioclase, which would be consistent with the low primary LREE abundances of bulk NWA 7325.

Figure 10 also shows data from feldspathic clasts in polymict ureilites, which show a large range of anorthite compositions and have various trace element abundances (Kita et al., 2004). The majority of these clasts contain albite-rich plagioclase with high incompatible trace element

571 abundances, and are interpreted to result from fractional crystallization of low-degree ureilitic
572 melts (Cohen et al., 2004; Kita et al., 2004). However, as mentioned above, a small fraction of
573 these clasts have anorthite-rich plagioclase and very magnesian mafic minerals (Fig. 5), similar
574 to NWA 7325. Plagioclase in these magnesian anorthite-rich clasts shows trace element
575 abundances that are very similar to those of plagioclase in NWA 7325; i.e., enriched in Mg and
576 Sr, but depleted Fe, K, Ti, and Ba compared with other anorthite-rich plagioclase in achondrites.
577 Using trace element partition coefficients between plagioclase and melt (Bindemann et al.,
578 1998; Dohmen and Blundy, 2014), we estimated the abundance of Ti, K, Ba, and Sr in the parent
579 melt of NWA 7325 as was done with plagioclase in felsic clasts in polymict ureilites by Kita et
580 al. (2004). The estimated trace element abundances in the parent melt of NWA 7325 are very
581 similar to those calculated for the parent melt of magnesian anorthitic clast γ-8 in polymict
582 ureilite DaG 319, i.e., high Sr abundance (~45×CI) and sub-CI to CI level abundances (0.3-1×
583 CI) of Ti, K, and Ba (Table 4). Barrat et al. (2015) also concluded from bulk rock compositional
584 studies that NWA 7325 crystallized from a melt that was very poor in volatiles (alkali elements)
585 and incompatible trace elements. They reported a positive Eu anomaly compared to middle
586 REEs and estimated Eu enrichment of 14-23× CI in the parent melt, which is similar to that of Sr
587 estimated above.
588 As discussed in Kita et al. (2004), single stage melting of a chondritic precursor would not
589 produce a melt that is enriched in Sr compared to K and Ba. Sr, K, and Ba are mainly hosted in
590 plagioclase, in which Sr is compatible (D>1) and others are not (D<1). A partial melt from a
591 chondritic source would be either more enriched in K and Ba than Sr (at lower degrees of
592 melting when plagioclase remains in the solid phase), or equally enriched (at high degrees of
593 melting when plagioclase has been eliminated from the solid). While to some degree the low K
594 abundance in the estimated parent melt could be due to the volatile-poor nature of the NWA
595 7325 parent asteroid, the low abundance of Ba still needs to be explained because of its
596 refractory nature. An incompatible trace element depleted source could be produced either by
597 repeated extraction of a low-degree partial melt that is enriched in these trace elements (i.e.,
598 near-fractional melting), or by a multi-stage igneous history .
599 Both Barrat et al. (2015) and Koefoed et al. (2016) discussed possible multi-stage histories
600 for NWA 7325, based on the positive $\delta^{26}Mg^*$ intercept of its Al-Mg isochron (Dunlap et al.,
601 2014; Koefoed et al., 2016). In these models, the parent melt of NWA 7325 formed by remelting

of its source region ~2.5-3 Ma after the initial differentation of the source (at < 1.8 Ma after CAI; Koefoed et al., 2016). Barrat et al. (2015) argued that the remelting could have been due to total impact melting of a gabbroic source. Although a discussion of these models is beyond the scope of this paper, we do note that the remelting event now evidenced in NWA 7325 by the internal textures of plagioclase (and argued to be due to impact in section 4.3.1), clearly involved only partial, not total remelting (principally of plagioclase and sulfide). Therefore, if the total impact remelting model of Barrat et al. (2015) is correct, then the partial remelting now seen in NWA 7325 must have occurred after the total remelting and would be a tertiary (rather than secondary) event.

4.5. Oxygen, Cr, and Ti Isotope Systematics and the Provenance of NWA 7325

Clayton and Mayeda (1996) first demonstrated that oxygen three-isotope systematics of achondrites can be used to distinguish groups of achondrites that may be (though are not necessarily) genetically related. Combining oxygen isotope data with Cr and Ti stable isotope anomalies (due to nucleosynthetic processes) can provide additional insights into genetic relationships among planetary materials (e.g., Warren, 2011a,b).

NWA 7325 has a negative $\Delta^{17}O$ value that is within both the small range of $\Delta^{17}O$ of acapulcoites and the larger range of $\Delta^{17}O$ of ureilites (Fig. 9b, 11). Its $\delta^{18}O$ value, however, is significantly higher than that of any acapulcoite (by almost 3‰) and similar to $\delta^{18}O$ values of ureilites of similar $\Delta^{17}O$; i.e., like ureilites, NWA 7325 plots on the CCAM array on a three oxygen-isotope diagram (Fig. 9).

Both $\varepsilon^{54}Cr$ and $\varepsilon^{50}Ti$ values of NWA 7325 exhibit deficits relative to terrestrial composition, as is observed for ordinary chondrites and most achondrites, including acapulocites and ureilites (Fig. 11). While $\Delta^{17}O$ of NWA 7325 falls within the range observed in ureilites, $\varepsilon^{54}Cr$ clearly sets NWA 7325 apart from all analyzed ureilites (green shaded region in Fig. 11a). The mean values in $\varepsilon^{50}Ti$-$\Delta^{17}O$ isotope space (Fig. 11b) show similar offsets from the ureilites, although the uncertainties associated with $\varepsilon^{50}Ti$ permit some overlap with ureilite compositions. The separation of NWA 7325 from the ureilites is clearly seen in the $\varepsilon^{54}Cr$-$\varepsilon^{50}Ti$ plot (Fig. 11c). In contrast, there is no resolvable difference between NWA 7325 and acapulcoites on these diagrams.

Archer et al. (2015) suggested that NWA 7325 experienced late addition of ~0.25% of a chondritic component, based on abundances of highly siderophile elements (HSE). We have examined the possibility that the Cr-Ti-O isotope compositions of NWA 7325 were offset from the ureilite field by addition of a chondritic component. Based on a mixing calculation shown in Table 7 and Fig. 11, the percentage of various chondritic compositions required to add to ureilites to bring them to the Cr-Ti-O isotopic compositions of NWA 7325 are: 31-52% H chondrite; 21-47% L chondrite; 10-34% CI chondrite; 11-29% CM chondrite; 11-20% CV chondrite; 13-20% CO chondrite; 8-20% CR chondrite; and 20-65% EH chondrite. The calculation considers the range of ureilite compositions shown in the green square (Fig. 11), as well as the error bars of the NWA 7325 data point. The calculated fractions are way too high to be compatible with the potential HSE evidence for chondritic mixing. We can thus rule out the possibility that mixing with a chondritic component is responsible for the deviation of NWA 7325 from the ureilite field in Fig. 11, and reiterate that NWA 7325 is clearly resolved from ureilites but not from acapulcoites on this diagram.

Based on these combined data for oxygen, chromium and titanium isotopes, as well as constraints from petrology, we consider two models for the provenance of NWA 7325.

4.5.1. Model 1- Accretion of the NWA 7325 parent body in the inner solar system from a reservoir similar to that of acapulcoites in $\Delta^{17}O$, $\varepsilon^{54}Cr$ and $\varepsilon^{50}Ti$.

Warren (2011a,b) pointed out that solar system materials fall into two distinct groups on plots of $\varepsilon^{54}Cr$ (or $\varepsilon^{50}Ti$) vs. $\Delta^{17}O$ (e.g., Fig. 11). The carbonaceous chondrites, Eagle Station pallasites, and an increasing number of CR-, CK- and CV-like ungrouped achondrites (Sanborn et al., 2013, 2014, 2015; Williams et al., 2016) form one group, which shows positive $\varepsilon^{54}Cr$ and $\varepsilon^{50}Ti$ values. Earth, Moon, ordinary chondrites, and most of the major differentiated meteorites (HED, angrites, aubrites,acapulcoites, ureilites, main group pallasites, mesosiderites and IIAB irons) form the second group, which shows zero or negative $\varepsilon^{54}Cr$ and $\varepsilon^{50}Ti$ values. A common interpretation of this bimodality (e.g., Warren, 2011a,b) is that it corresponds to inner solar system (Earth, Moon, OC, achondrites) vs. outer solar system (CC) materials. If this interpretation is correct, then NWA 7325 and acapulcoites (as well as ureilites) must have formed in the inner asteroid belt, and the NWA 7325 parent body may have accreted from the same reservoir of materials (in terms of $\varepsilon^{54}Cr$, $\varepsilon^{50}Ti$ and $\Delta^{17}O$) as acapulcoites.

663 However, this model would also have to account for the large difference in $\delta^{18}O$ between
664 NWA 7325 and acapulcoites (Fig. 9b). This difference is too large to be a result of igneous
665 evolution, because mass dependent oxygen isotope fractionation factors at magmatic
666 temperatures are very small (Eiler, 2001; Valley et al., 2014). For example, the plagioclase-rich
667 achondrite GRA 06128/06129 has been suggested to be a crustal cumulate complimentary to
668 brachinites or brachinite-like primitive achondrites, and yet its $\delta^{18}O$ value is nearly identical to
669 that of most brachinites (Shearer et al., 2010; Day et al., 2012). Another possibility is that the
670 difference in $\delta^{18}O$ between acapulcoites and NWA 7325 is due to pre-igneous aqueous alteration
671 on the NWA 7325 parent body, as suggested by Greenwood et al. (2012) to explain mass-
672 dependent fractionation among winonaites. Although inner solar system bodies are generally
673 thought to have accreted with little or no water ice, it is possible that the NWA 7325 parent body
674 accreted later than acapulcoites, after the snow line had moved inward toward the Sun. In this
675 case, the $\Delta^{17}O$ of the water ice must have been very similar to that of the anhydrous rock.
676 Recently, Barrat et al. (2016) reported anomalies observed in the Tm isotopic composition
677 among Solar System materials. Among the meteorite groups analyzed by Barrat et al. (2016),
678 objects such as Earth, Mars, and Vesta exhibited a relatively consistent Tm/Tm^* value of less
679 than 1, while carbonaceous chondrites predominately had Tm/Tm^* values greater than 1. The
680 Tm/Tm^* value for NWA 7325 reported in this same study was the lowest Tm/Tm^* value of any
681 of the meteorites measured. The observed Tm/Tm^* anomaly, coupled with the negative $\varepsilon^{54}Cr$
682 and $\varepsilon^{50}Ti$, may provide an additional line of evidence for formation in the inner Solar System
683
684 *4.5.2. Model 2- Accretion of the NWA 7325 parent body in the outer asteroid belt or outer solar*
685 *system, beyond the snow line.*
686 Alternatively, the $\delta^{18}O$ value of NWA 7325 (i.e., its location on the CCAM array in three-
687 oxygen isotope space) may indicate that the NWA 7325 parent body accreted in the outer solar
688 system. This model is suggested by the hypothesis that oxygen isotope compositions on the
689 CCAM line are a result of parent body aqueous alteration of originally anhydrous primitive
690 materials (Young and Russell, 1998; Young et al. 1999; Kita et al., 2011; Rudraswami et al.,
691 2011). We briefly summarize the basis for this interpretation.
692 Most achondrite bulk oxygen isotope ratios plot significantly to the left of the CCAM line on
693 an oxygen three isotope diagram, with the exception of NWA 7325 and ureilites (Fig. 9). Many

694 of them, especially primitive achondrites that have experienced only low degrees of igneous
695 processing (e.g., acapulcoites, lodranites, brachinites) plot near the Primitive Chondrule Mineral
696 (PCM) line, which is a slope ~1.0 regression line for the oxygen isotope ratios of olivine and
697 pyroxene in pristine chondrules from the very primitive (type 3.00) Acfer 094 ungrouped
698 carbonaceous chondrite (Ushikubo et al., 2012). Oxygen isotope compositions of chondrules in
699 the least metamorphosed carbonaceous chondrites all plot along the PCM line (Rudraswami et
700 al., 2011; Tenner et al., 2013, 2015), and therefore this line has been argued to represent the
701 primordial trend of oxygen isotope compositions in the Solar System (Rudraswami et al., 2011;
702 Ushikubo et al., 2012; Tenner et al., 2013, 2015). In contrast to materials near the PCM line, the
703 oxygen isotope compositions of most bulk carbonaceous chondrites are shifted to the right (to
704 higher $\delta^{18}O$), and plot along or near the CCAM line. A number of recent studies have shown
705 that this shift could have resulted from oxygen isotope exchange between ^{16}O-rich silicates (low
706 $\Delta^{17}O$) and ^{16}O-poor fluids (high $\Delta^{17}O$) originally located along the PCM line in carbonaceous
707 chondrite parent bodies (e.g., Young and Russell, 1998; Young et al. 1999; Kita et al., 2011;
708 Rudraswami et al., 2011). Obviously, this interpretation requires that the carbonaceous chondrite
709 parent bodies accreted with abundant water ice, i.e., in the outer solar system beyond the snow
710 line (Ciesla and Cuzzi, 2006).
711 The observation that the oxygen isotope composition of NWA 7325 (and also compositions
712 of ureilites) plots on the CCAM line may indicate that the parent body of NWA 7325 (and that of
713 ureilites) formed in the outer asteroid belt beyond the snow line, thus accreting with a significant
714 amount of water-ice and experiencing pre-igneous aqueous alteration. If this is correct, then the
715 observation that NWA 7325 has $\Delta^{17}O$ similar to that of acapulcoites would not be indicative of
716 any genetic relationship, since acapulcoites would have formed in the inner solar system belt,
717 inside the snow line.
718 This model for the provenance of NWA 7325 would also have to account for the grouping of
719 NWA 7325 and ureilites with inner solar system materials (OC and most achondrites), rather
720 than outer solar system materials (aqueously altered CC), on $\varepsilon^{54}Cr$ or $\varepsilon^{50}Ti$ vs. $\Delta^{17}O$ diagrams
721 (Fig. 11). This could be explained if the dichotomy between the two groups seen in Fig. 11 is
722 not exclusively spatial, but has a temporal component as well. Leya et al. (2008) suggested that
723 carbonaceous chondrites acquired their distinct mix of nucleosynthetic components as a result of
724 formation later than other meteorites. Dauphas et al. (2010) suggested that planetary materials

incorporated different amounts of ^{54}Cr anomaly-bearing particles due to late injection into "selective" regions by a supernova. Very early accretion times (<1 Ma after CAI) have been inferred for the parent bodies of some differentiated meteorites (including ureilites) from Hf-W age dating and thermal modeling (Bizzarro et al., 2005; Kleine et al., 2005; Hevey and Sanders, 2006; Markowski et al., 2006; Wilson et al., 2008). These accretion times are earlier than the ages of most analyzed chondrules, and therefore earlier than the accretion of most carbonaceous chondrite parent bodies (Fujiya et al., 2012; Nagashima et al., 2014). This suggests the possibility that the parent bodies of NWA 7325 and the ureilites accreted in the solar system before ^{54}Cr and ^{50}Ti anomalies were introduced to this region. In this case, the identical Cr and Ti isotope compositions of NWA 7325 and acapulcoites would not be indicative of formation from a spatially common reservoir.

5. SUMMARY

Ungrouped achondrite NWA 7325 is a protogranular to poikilitic-textured assemblage of 10-15 vol. % Mg-rich olivine (Fo 98), 25-30 vol. % diopside (Wo 45, Mg# 98), 55-60 vol. % Ca-rich plagioclase (An 90), and trace amounts of Cr-rich sulfide and Fe,Ni metal. In terms of modal mineralogy and mineral compositions it is unique compared with all known meteoritic materials other than a rare feldspathic lithology found as clasts ("the magnesian anorthitic lithology") in polymict ureilites. In agreement with previous investigations, we interpret NWA 7325 to be a cumulate rock that crystallized at temperatures ≥1200 °C and conditions of very low oxygen fugacity from a generally basaltic, incompatible element-depleted melt. Trace element abundances in plagioclase indicate that this melt could only have formed by fractional (not batch) melting of a chondritic source, or a multi-stage igneous history. NWA 7325 experienced a subsequent event (argued to be impact and excavation), in which plagioclase was substantially remelted and recrystallized with a distinct texture.

The oxygen isotope composition of NWA 7325 plots in the range of ureilites on the CCAM line and is identical, within error, to the composition of the two analyzed clasts of the magnesian anorthitic lithology in polymict ureilites. It plots near a slope ~0.5 mass fractionation line extended to higher δ^{18}O from acapulcoites. In terms of ε^{54}Cr and ε^{50}Ti values, NWA 7325 exhibits deficits relative to the terrestrial standard, as observed for ordinary chondrites and most

achondrites, including ureilites. Its ε^{54}Cr value is distinct from that of any analyzed ureilite, but is not resolved from that of acapulcoites.

NWA 7325 is derived from a parent body that has not previously been sampled by any known meteorite. However, rare clasts of a magnesian anorthitic lithology in polymict ureilites show mineral assemblages, textures, and compositions (including oxygen isotope compositions) that are strikingly similar to NWA 7325. These clasts may be xenoliths derived from the NWA 7325 parent body, and merit further investigation. We discuss two possible models for the provenance of the NWA 7325 parent asteroid: 1) accretion in the inner solar system from the same reservoir of Cr, Ti and O isotopes as acapulcoites; 2) early accretion (<1 Ma after CAI) in the outer solar system (beyond the snow line), before ^{54}Cr and ^{50}Ti anomalies were introduced to this region. The mid-IR emission spectrum obtained in this work from a polished slab of NWA 7325 can be compared in the future with spectra of new meteorites or asteroids/planets to help identify similar materials and/or the parent body of this meteorite.

ACKNOWLEDGMENTS

The authors thank Brian Hess for the preparation of the polished thin section and epoxy mount of NWA 7325, Travis Tenner and Jim Kern for assistance with SIMS instrumentation, Michael Jercinovic for assistance with SEM and EMPA at the University of Massachusetts (Amherst), and D. Kent Ross for assistance with EMPA at ARES, JSC. We also thank to Dr. Tim Glotch for the use of his lab at Stony Brook University to acquire emissivity spectra, and Dr. Iris Weber for providing her thin-section reflectance spectrum. We thank Kurt Marti for providing the Acapulco sample for Cr and Ti isotope measurements. Helpful reviews from Jean-Alix Barrat, two anonymous reviewers, and the associate editor, Sara Russell, as well as enlightening discussions with Allan Treiman, are greatly appreciated. WiscSIMS is partly supported by NSF (EAR03-19230, EAR13-55590). This work was supported by NASA grants NNX12AH74G (CG), NNX11AG62G (NK), NNX14AM62G (QZY), and the Lunar and Planetary Instititute (University Space Resources Association). QZY also acknowledges the UC Office of the President (UC Lab Fees Award ID# 12-LR-237921) for partial support of this work. This paper is PSI contribution No. 630 and LPI contribution #xxxx.

REFERENCES

Amelin Y., Koefoed P., Iizuka T. and Irving A. J. (2013) U-Pb age of ungrouped achondrite NWA 7325. In *48th Annual Meteoritical Society Meeting, #5165 (abstr.).*

Anders E. and Grevesse N. (1989) Abundances of the elements: meteoritic and solar. *Geochim. Cosmochim. Acta* **53**, 197-214.

Archer G. J., Walker R. J. and Irving A. J. (2015) Highly siderophile element and ^{187}Re-^{187}Os isotopic systematics of ungrouped achondrite Northwest Africa 7325. In *46th Lunar. Planet. Sci. Conf., #1987 (abstr.).*

Ashley J. W. (2011) Meteorites on Mars as Planetary Research Tools with Special Considerations for Martian Weathering Processes. PhD Dissertation. Arizona State University.

Barrat J. A., Greenwood R. C., Verchovsky A. B., Gillet Ph., Bollinger C., Langlade J. A., Liorzou C. and Franchi I. A. (2015) Crustal differentiation in the early solar system: clues from the unique achondrite Northwest Africa 7325 (NWA 7325). *Geochim. Cosmochim. Acta* **168**, 280-292.

Barrat J. A., Dauphas N., Gillet P., Bollinger C., Etoubleau J., Bischoff A. and Yamaguchi A. (2016) Evidence from Tm anomalies for non-CI refractory lithophile element proportions in terrestrial planets and achondrites. *Geochim. Cosmochim. Acta* **176**, 1–17.

Bindeman I. N., Davis A. M. and Drake M. J. (1998) Ion microprobe study of plagioclase-basalt partition experiments at natural concentration levels of trace elements. *Geochim. Cosmochim. Acta* **62**, 1175–1193.

Bischoff A. , Horstmann M., Barrat J-A., Chaussidon M., Pack A. and Herwatz D. (2014) Trachyandesitic volcanism in the early Solar System. *Proc. Nat. Acad. Sci.* **111**, 12689-12692.

Bizzarro M., Baker A., Haack H. and Lundgaard K. L. (2005) Rapid timescales for accretion and melting of differentiated planetesimals inferred from ^{26}Al-^{26}Mg chronometry. *Astrophys. Jour.* **632**, L41-L44.

Burroni A. and Folco L. (2008) Frontier Mountain meteorite specimens of the acapulcoite-lodranite clan: petrography, pairing, and parent-rock lithology of an unusual intrusive rock. *Meteorit. Planet. Sci.* **43**, 731-744.

Christensen, P. R., Bandfield J. L., Hamilton V. E., Howard D. A., Lane M. D., Piatek J. L., Ruff S. W. and Stefanov W. L. (2000) A thermal emission spectral library of rock-forming minerals. *Jour. Geophys. Res.* **105**, 9735-9739.

Ciesla F. J. and Cuzzi J. N. (2006) The evolution of the water distribution in a viscous protoplanetary disk. *Icarus* **181**, 178-204.

Clayton R. N. and Kieffer S. W. (1991) Oxygen isotopic thermometer calibrations. In Stable isotope geochemistry: A Tribute to Samuel Epstein, edited by Taylor H. P. Jr., O'Neil J. R., and Kaplan I. R. Geochemical Society (Special Publication No. 3). pp. 3–10.

Clayton R. N. and Mayeda T. K. (1996) Oxygen isotope studies of achondrites. *Geochim. Cosmochim. Acta* **60**, 1999–2017.

Clayton R. N. and Mayeda T. K. (2009) Kinetic Isotope Effects in Oxygen in the Laboratory Dehydration of Magnesian Minerals. *Jour. Phys. Chem. A* **113**, 2212-2217.

Clayton R. N., Onuma N., Grossman L. and Mayeda T. K. (1977) Distribution of pre-solar component in Allende and other carbonaceous chondrites. *Earth Planet. Sci. Lett.* **34**, 209–224.

Clayton R. N., Mayeda T. K. and Rubin A. E. (1984) Oxygen isotopic compositions of enstatite chondrites and aubrites. *Jour. Geophys. Res.* **89**, C245-249.

Clayton R. N., Mayeda T. K., Goswami J. N. and Olsen E. J. (1991) Oxygen isotope studies of ordinary chondrites. *Geochim. Cosmochim. Acta* **55**, 2317-2337.

Cohen B. A., Goodrich C. A. and Keil K. (2004) Feldspathic clast populations in polymict ureilites: stalking the missing basalts from the ureilite parent body. *Geochim. Cosmochim. Acta* **68**, 4249-4266.

Dauphas N., Remusat L., Chen J. H., Roskosz M., Papanastassiou D. A., Stodolna J., Guan Y., Ma C. and Eiler J. M. (2010). Neutron-rich chromium isotope anomalies in supernova nanoparticles. *Astrophys. Jour.* **720**, 1577–1591.

Day J. M. D., Walker R. J., Ash R. D., Liu Y., Rumble D., III, Irving A. J., Goodrich C. A., Tait K., McDonough W. F. and Taylor L. A. (2012) Origin of felsic achondrites Graves Nunataks 06128 and 06129, and ultramafic brachinites and brachinite-like achondrites by partial melting of volatile-rich primitive parent bodies. *Geochim. Cosmochim. Acta* **81**, 94–128.

Day J. M. D., Corder C. A., Rumble D. III, Assayag N., Cartigny P. and Taylor L.A. (2015) Differentiation processes in FeO-rich asteroids revealed by the achondrite Lewis Cliff 88763. *Meteorit. Planet. Sci.* **50**, 1750-1766.

Delaney J. S., Zanda B., Clayton R. N. and Mayeda T. (2000) Zag(b): a ferroan achondrite intermediate between brachinites and lodranites. In *31st Lunar Planet. Sci. Conf., #1745 (abstr.)*.

Dohmen R. and Blundy J. (2014) A predictive thermodynamic model for element partitioning between plagioclase and melt as a function of pressure, temperature and composition. *American J. Sci.* **314**, 1319-1372.

Downes H., Mittlefehldt D. W., Kita N. T. and Valley J. W. (2008) Evidence from polymict ureilite meteorites for a disrupted and re-accreted single ureilite parent asteroid gardened by several distinct impactors. *Geochim. Cosmochim. Acta* **72**, 4825-4844.

Dunlap D. R., Wadhwa M. and Romaneillo S. R. (2014) ^{26}Al-^{26}Mg systematics in the unusual ungrouped achondrite NWA 7325 and the eucrite Juvinas. In *45th Lunar Planet. Sci. Conf., #2186 (abstr.)*.

Eiler J. M. (2001). Oxygen isotope variations of basaltic lavas and upper mantle rocks. In: Valley, J. W. & Cole, D. R. (eds) Stable Isotope Geochemistry. Mineralogical Society of America and Geochemical Society, Reviews in Mineralogy and Geochemistry **43**, 319-364.

Floss C., Crozaz G., McKay G. Mikouchi T. and Killgore M. (2003) Petrogenesis of angrites. *Geochim. Cosmochim. Acta* **67**, 4775-4789.

Floss C., Taylor L. A., Promprated P. and Ruble D. III. (2005) Northwest Africa 011: A "eucritic" basalt from a non-eucrite parent body. *Meteorit. Planet. Sci.* **40**, 343-360.

Fujiya W., Sugiura N., Hotta H., Ichimura K. and Sano Y. (2012) Evidence for the late formation of hydrous asteroids from young meteoritic carbonates. *Nat. Commun.* **3**, 627.

Hevey P. J. and Sanders I. S. (2006) A model for planetesimal meltdown by ^{26}Al and its implications for meteorite parent bodies. *Meteorit. Planet. Sci.* **41**, 95-106.

Gardner-Vandy K. G. (2012) Partial melting on FeO-rich asteroids: insights to the first stage of planetary differentiation. PhD Dissertation. University of Arizona.

Gardner-Vandy K. G., Lauretta D. S., Greenwood R. C., McCoy T. J. and Killgore M. (2012) The Tafassasset primitive achondrite: insights into initial stages of planetary differentiation. *Geochim. Cosmochim. Acta* **85**, 142-159.

Gardner-Vandy K. G., Lauretta D. S. and McCoy T. J. (2013) A petrologic, thermodynamic and experimental study of brachinites: partial melt residues of an R chondrite-like precursor. *Geochim. Cosmochim. Acta* **122**, 36-57.

Goodrich C. A. and Delaney J. S. (2000) Fe/Mg-Fe/Mn relations of meteorites and primary heterogeneity of primitive achondrite parent bodies. *Geochim. Cosmochim. Acta* **64**, 2255–2273.

Goodrich C. A. and Righter K. (2000) Petrology of Unique Achondrite QUE 93148. A Piece of the HED Mantle? *Meteorit. Planet. Sci.* **35**, 521-535.

Goodrich C. A. and Wilson L. (2014) Feldspathic clast populations in polymict ureilites: determining the compositions of melts and the mode of melt extraction on the ureilite parent body. In *45th Lunar Planet. Sci. Conf., #1342 (abstr.).*

Goodrich C. A., Scott E. R. D. and Fioretti A. M. (2004) Ureilitic breccias: clues to the petrologic structure and impact disruption of the ureilite parent body. *Chemie der Erde* **64**, 283–327.

Goodrich C. A., Wlotzka F., Ross D. K. and Bartoschewitz R. (2006) Northwest Africa 1500: plagioclase-bearing monomict ureilite or ungrouped achondrite? *Meteorit. Planet. Sci.* **41**, 925-952.

Goodrich C. A., Van Orman J. A. and Wilson L. (2007) Fractional melting and smelting on the ureilite parent body. *Geochim. Cosmochim. Acta* **71**, 2876–2895.

Goodrich C. A., Fioretti A. M. and Van Orman J. A. (2009) Petrogenesis of augite-bearing ureilites Hughes 009 and FRO 90054/93008 inferred from melt inclusions in olivine, augite and orthopyroxene. *Geochim. Cosmochim. Acta* **73**, 3055-3076.

Goodrich C. A., Kita N. T., Spicuzza M. J., Valley J. W., Zipfel J., Mikouchi T. and Miyamoto M. (2011) The Northwest Africa 1500 meteorite: not a ureilite, maybe a brachinite. *Meteorit. Planet. Sci.* **45**, 1906-1928.

Goodrich C. A., Ash R. D., Van Orman J. A., Domanik K. and McDonough W. F. (2013) Metallic phases and siderophile elements in main group ureilites: Implications for ureilite petrogenesis. *Geochim. Cosmochim. Acta* **112**, 340-373.

Goodrich C. A., Harlow G., Van Orman J. A., Sutton S. R., Jercinovic M. J. and Mikouchi T. (2014) Petrology of chromite in ureilites: deconvolution of primary oxidation states and secondary reduction processes. *Geochim. Cosmochim. Acta* **135**, 126-169.

Goodrich C. A., Kita N. T., Sutton S. R., Wirick S. and Gross J. (2015) The Miller Range 090340 and 090206 meteorites: Identification of new brachinite-like achondrites with implications for the diversity and petrogenesis of the brachinite clan. *Meteorit. Planet. Sci., submitted in revised form.*

Goodrich C.A., Ebert S., Bischoff A., Treiman A.H., Pack A. and Barrat J.-A. (2016a) MS-MU-012: A primary plagioclase-bearing main group ureilite from Almahata Sitta, with implications for the igneous evolution of the ureilite parent body. In *79th Annual Meeting of the Meteoritical Society, #6105 (abstr.).*

Goodrich C. A., Treiman A. H., Kita N. T. and Defouilloy C. (2016b) Increasing diversity of ordinary chondrite and Rumuruti-type chondrites clasts in polymict ureilites. In *47th Lunar Planet Sci. Conf., #1617 (abstr.).*

Greenwood R. C., Franchi I. A., Gibson J. M. and Benedix G. K. (2012) Oxygen isotope variation in primitive achondrites: the influence of primordial, asteroidal and terrestrial processes. *Geochim. Cosmochim. Acta* **94**, 146-163.

Horstmann M. and Bischoff A. (2014). The Almahata Sitta polymict breccia and the late accretion of asteroid 2008 TC_3. *Chemie der Erde* **74**,149-183.

Hsu W. And Crozaz G. (1996) Mineral chemistry and the petrogenesis of eucrites: I. Noncumulate eucrites. *Geochim. Cosmochim. Acta* **60**, 4571-4591.

Hsu W. And Crozaz G. (1997) Mineral chemistry and the petrogenesis of eucrites: II. Cumulate eucrites. *Geochim. Cosmochim. Acta* **61**, 1293-1302.

Hunter R. H. (1996) Texture development in cumulate rocks. *In* Layered Intrusions (R.G. Cawthorn, ed.) Elsevier.

Ikeda Y., Prinz M. and Nehru C. E. (2000) Lithic and mineral clasts in the Dar al Gani (DaG) 319 polymict ureilite. *Antarctic Meteorite Research* **13**, 177–221.

Irving A. J. , Tanaka R., Steele A., Kuehner S. M., Bunch T. E., Wittke J. H. and Hupe G. M. (2011) Northwest Africa 6704: A unique cumulate permafic achondrite containing sodic feldspar, awaruite and "fluid" inclusions, with an oxygen isotopic composition in the acapulcoite-lodranite field. In *46th Annual Meeting of the Meteoritical Society*, *#5231 (abstr.).*

Irving A. J., Kuehner S. M., Bunch T. E., Ziegler K., Chen G., Herd C. D. K., Conrey R. M. and Ralew S. (2013) Petrology and oxygen isotopic composition of brachinite-like achondrites

Northwest Africa 7399 and Northwest Africa 7605, and evidence for late-stage methane-triggered reduction. In *44th Lunar and Planet. Sci. Conf.*, *#2164 (abstr.)*.

Jabeen I., Ali A., Banerjee N. R., Osinski G. R., Ralew S. and DeBoer S. (2014) Oxygen isotope compositions of mineral separates from NWA 7325 suggest a planetary (Mercury?) origin. In *45th Lunar Planet. Sci. Conf.*, *#2215 (abstr.)*.

Jenniskens P., Fries M. D., Yin Q.-Z., Zolensky M., Krot A. N., Sandford S. A., Sears D., Beauford R., Ebel D. S., Friedrich J. M., Nagashima K., Wimpenny J., Yamakawa A., Nishiizumi K., Hamajima Y., Caffee M. W., Welten K. C., Laubenstein M., Davis A. M., Simon S. B., Heck P. R., Young E. D., Kohl I. E., Thiemens M., Nunn M. H., Mikouchi T., Hagiya K., Ohsumi K., Cahill T. A., Lawton J. A., Barnes D., Steele A., Rochette P., Verosub K., Gattacceca J., Cooper G., Glavin D. P., Burton A. S., Dworkin J. P., Elsila J. E., Pizzarello S., Ogliore R., Schmitt-Kopplin P., Harir M., Hertkorn N., Verchovsky A., Grady M., Nagao K., Okazaki R., Takechi H., Hiroi T., Smith K., Silber E. A., Brown P. G., Albers J., Klotz D., Hankey M., Matson R., Fries J. A., Walker R. J., Puchtel I., Lee C.-T. A., Erdman M. E., Eppich G. R., Roeske S., Gabelica Z., Lerche M., Nuevo M., Girten B. and Worden S. P. (2012) Radar enabled recovery of the Sutter's Mill meteorite, a carbonaceous chondrite regolith breccia. *Science* **338**, 1583-1587.

Jenniskens P., Rubin A. E., Yin Q.-Z., Sears D. W. G., Sandford S. A., Zolensky M. E., Krot A. N., Blair L., Kane D., Utas J., Verish R., Friedrich J. M., Wimpenny J., Eppich G. R., Ziegler K., Verosub K. L., Rowland D. J., Albers J., Gural P. S., Grigsby B., Fries M. D., Matson R., Johnston M., Silber E., Brown P., Yamakawa A., Sanborn M. E., Laubenstein M. Welten K. C., Nishiizumi K., Meier M. M. M., Busemann H., Clay P., Caffee M. W., Schmitt-Kopplin P., Hertkorn N., Glavin D. P., Callahan M. P., Dworkin J. P., Wu Q., Zare R. N., Grady M., Verchovsky S., Emel'yanenko V., Naroenkov S., Clark D. L., Girten B. and Worden P. S. (The Novato Meteorite Consortium) (2014) Fall, recovery, and characterization of the Novato L6 chondrite breccia. *Meteorit. Planet. Sci.* **49**, 1388-1425.

Keil K. (2007) Occurrence and origin of keilite, (Fe>0.5,Mg<0.05)S, in enstatite chondrite impact-melt rocks and impact-melt breccias. *Chemie der Erde* **67**, 37-54.

Keil K. (2012) Angrites, a small but diverse suite of ancient, silica-undersaturated volcanic-plutonic mafic meteorites, and the history of their parent asteroid. *Chemie der Erde* **72**,191-218.

Kimura M., Tsuchiyama A., Fukuoka T. and Iimura Y. (1992) Antarctic primitive achondrites Yamato-74025, -75300, and -75305: Their mineralogy, thermal history, and the relevance to winonaite. Proceedings, National Institute of Polar Research Symposium on Antarctic Meteorites **5**, 165-190.

Kita N. T., Ikeda Y., Togashi S., Liu Y., Morishita Y. and Weisberg M. K. (2004) Origin of ureilites inferred from a SIMS oxygen isotopic and trace element study of clasts in the Dar al Gani 319 polymict ureilite. *Geochim. Cosmochim. Acta* **68**, 4213–4235.

Kita N. T., Nagahara H., Tachibana S., Tomomura S., Spicuzza M. J., Fournelle J. H. and Valley J. W. (2010) High precision SIMS oxygen three isotope study of chondrules in LL3 chondrites: Role of ambient gas during chondrule formation. *Geochim. Cosmochim. Acta* **74**, 6610–6635.

Kita N. T., Ushikubo T., Knight K. B., Mendybaev R. A., Davis A. M., Richter F. M., Nakashima D., Spicuzza M. J. and Valley J. W. (2011) High precision oxygen isotope systematics of a Type B1 CAI from Leoville (CV3). In *46th Annual Meeting of the Meteoritical Society*, *#5094 (abstr.)*.

Kleine T., Mezger K., Palme H., Scherer E. and Münker C. (2005) Early core formation in asteroids and late accretion of chondrite parent bodies: evidence from ^{182}Hf-^{182}W in CAIs, metal-rich chondrites, and iron meteorites. *Geochim. Cosmochim. Acta* **69**, 5815-5818.

Koefoed P., Amelin Y., Yin Q.-Z., Wimpenny J., Sanborn M. E., Iizuka T. and Irving A. J. (2016) U-Pb and Al-Mg systematics of the ungrouped achondrite Northwest Africa 7325. *Geochim. Cosmochim. Acta* **183**, 31–45.

Köhler T. P. and Brey G. P. (1990) Calcium exchange between olivine and clinopyroxene calibrated as a geothermobarometer for natural peridotites from 2 to 60 kb with applications. *Geochim. Cosmochim. Acta* **54**, 2375-2388.

Krot A. N., Keil K., Scott E. R. D., Goodrich C.A. and Weisberg M. K. (2013) Classification of meteorites and their genetic relationships. *In* Treatise on Geochemistry, Vol. 1, Meteorites and Cosmochemical Processes (Ed. A. M. Davis) 2nd Edition, p. 1-64

Lane M. D., Glotch T. D., Dyar M. D., Pieters C. M., Klima R., Hiroi T., Bishop J. L. and Sunshine J. (2011) Mid-infrared spectroscopy of synthetic olivines: thermal emission, specular and diffuse reflectance, and attenuated total reflectance studies of forsterite to fayalite. *Jour. Geophys. Res.* **116**, E08010.

Leya I., Schonbachler M. Wiechert U., Krahenbuhl U. and Halliday A. N. (2008) Titanium isotopes and the radial heterogeneity of the solar system. *Earth Planet. Sci. Lett.* **266**, 233-244.

Longhi J. (1991) Comparative liquidus equilibria of hypersthene-normative basalts at low pressure. *Am. Min.* **76**,785-800.

Markowski A., , Leya I., Quitté G., Ammon K., Halliday A. N. and Wieler R. (2006) Correlated helium-3 and tungsten isotopes in iron meteorites: quantitative cosmogenic corrections and planetesimal formation times. *Earth Planet. Sci. Lett.* **250,** 104-115.

Mittlefehldt D. W., Lindstrom M. M., Bogard D. D., Garrison D. H. and Fields S. W. (1996) Acapulco- and Lodran-like achondrites: Petrology, geochemistry, chronology, and origin. *Geochim. Cosmochim. Acta* **60**, 867-882.

Mittlefehldt D. W., McCoy T. J., Goodrich C. A. and Kracher A. (1998) Non-chondritic meteorites from asteroidal bodies. In *Planetary Materials*, edited by Papike J. J. Reviews in Mineralogy, vol. 36. Washington, D.C.: Mineralogical Society of America. pp. 4-1 to 4-195.

Mittlefehldt D. W., Bogard D. D., Berkley J. L. and Garrison D. (2003) Brachinites: igneous rocks from a differentiated asteroid. *Meteorit. Planet. Sci.* **38**, 1601-1625.

K. Nagashima, A. N. Krot and G. R. Huss (2014). ^{26}Al in chondrules from CR2 chondrites. *Geochemical Journal* **48**, 561-570.

Nehru C. E., Prinz M., Delaney J. S., Dreibus G., Palme H., Spettel B. and Wänke H. (1983) Brachina: a new type of meteorite, not a chassignite. Proceedings, 14th Lunar and Planetary Science Conference. *Journal of Geophysical Research* 88 (Suppl.): B237-B244.

Niederer F. R., Papanastassiou D. A. and Wasserburg G. J. (1985) Absolute isotopic abundances of Ti in meteorites. *Geochim. Cosmochim. Acta* **49**, 835-851.

Petaev M. I. Barsukova L. D., Lipschutz M. E., Wang M.-S., Ariskin A. A., Clayton R. N. and Mayeda T. K. (1994) The Divnoe meteorite: petrology, chemistry, oxygen isotopes and origin. *Meteorit. Planet. Sci.* **29**, 182-199.

Popova O. P., Jenniskens P., Emel'yanenko V., Kartashova A., Biryukov E., Khaibrakhmanov S., Shuvalov V., Rybnov Y., Dudorov A., Grokhovsky V. I., Badyukov D. D., Yin Q.-Z., Gural P. S., Albers J., Granvik M., Evers L. G., Kuiper J., Kharlamov V., Solovyov A., Rusakov Y. S., Korotkiy S., Serdyuk I., Korochantsev A. V., Larionov M. Y., Glazachev D., Mayer A. E., Gisler G., Gladkovsky S. V., Wimpenny J., Sanborn M. E., Yamakawa A.,

Verosub K., Rowland D. J., Roeske S., Botto N. W., Friedrich J. M., Zolensky M., Le L., Ross D., Ziegler K., Nakamura T., Ahn I., Lee J. I., Zhou Q., Li X.-H., Li Q.-L., Liu Y., Tang G.-Q., Hiroi T., Sears D., Weinstein I. A., Vokhmintsev A. S., Ishchenko A. V., Schmitt-Kopplin P., Hertkorn N., Nagao K., Haba M. K., Komatsu M. and Mikouchi T. (The Chelyabinsk Airburst Consortium). (2013) Chelyabinsk Airburst, Damage Assessment, Meteorite Recovery, and Characterization. *Science* **342**, 1069-1073.

Prinz M., Weisberg M. K., Nehru C. E. and Delaney J. S. (1986) North Haig and Nilpena: paired polymict ureilites with Angra dos Reis-related and other clasts. In *17th Lunar Planet. Sci.Conf.*, 681-682 (abstr.).

Prinz M., Weisberg M. K., Nehru C. E. and Delaney J. S. (1987a) EET 83309, a polymict ureilite: recognition of a new group. In *18th Lunar Planet. Sci. Conf.*, 802-803 (abstr.).

Prinz M., Weisberg M. K., Nehru C. E. and Delaney J. S. (1987b) Black inclusions of carbonaceous chondrite matrix material in polymict ureilites. *Meteoritics* **22**, 482-483 (abstr.).

Prinz M., Weisberg M. K. and Nehru C.E. (1986) Feldspathic components in polymict ureilites. *Lunar Planet. Sci.* **19**, 947-948 (abstr.).

Ramsey M. S. and Christensen P. R. (1998) Mineral abundance determination: Quantitative deconvolution of thermal emission spectra. *Jour. Geophys. Res.* **103**, 577-596.

Rudraswami N. G., Ushikubo T., Nakashima D. and Kita N. T. (2011) Oxygen isotope systematics of chondrules in Allende CV3 chondrite: High precision ion microprobe studies. *Geochim. Cosmochim. Acta* **75**, 7596-7611.

Ruzicka A., Grossman J., Bouvier A., Herd C. D. K. and Agee C. B. (2015) The Meteoritical Bulletin, No 101. *Meteorit. Planet. Sci.* **50**, 1661-1800.

Sanborn M. E., Yamakawa A., Yin Q. -Z., Irving A. J. and Amelin Y. (2013) Chromium isotopic studies of ungrouped achondrites NWA 7325, NWA 2976 and NWA 6704. In *76th Annual Meeting of the Meteoritical Society*, *#5220 (abstr.).*

Sanborn M. E., Yin Q.-Z. and Irving A. J. (2014) Isotope forensics utilizing Δ^{17}O-ε^{54}Cr systematics provide supporting evidence for differentiated parent bodies overlain by chondritic veneers: A case for the CR parent body. In *45th Lunar Planet. Sci. Conf., #2032 (abstr.).*

Sanborn M. E., Yin Q.-Z., Irving A. J. and Bunch T. E. (2015) Differentiated planetesimals with chondritic crusts: new Δ^{17}O-ε^{54}Cr evidence in unique, ungrouped achondrites for partial melting of the CV/CK and CO parent bodies. In *46th Lunar Planet. Sci. Conf., #2259 (abstr.)*.

Schiller M., Baker J. A., and Bizzarro M. (2010) ^{26}Al-^{26}Mg dating of asteroidal magmatism in the young Solar System. *Geochim. Cosmochim. Acta* **74**, 4844-4864.

Scott E. R. D., Greenwood R. C., Franchi I. A. and Sanders I. S. (2009) Oxygen isotopic constraints on the origin and parent bodies of eucrites, diogenites, and howardites. *Geochim. Cosmochim. Acta* **73**, 5835-5853.

Shearer C. K., Burger P. V., Karner J., Wadhwa M., Gaffney A., Shafer J., Geissman J., Atudorei N-V., Herd C., Weiss B. P., King P. L., Crowther S. A. and Gilmour J. D. (2010) Non-basaltic asteroidal magmatism during the earliest stages of solar system evolution: A view from Antarctic achondrites Graves Nunatak 06128 and 06129. *Geochim. Cosmochim. Acta* **74**, 1172-1199.

Shields W. R., Murphy T. J., Catanzaro E. J. and Garner E. L. (1966) Absolute isotopic abundance ratios and the atomic weight of a reference sample of chromium. *Journal of Research of the National Bureau of Standards* **70A**, 193-197.

Shukolyukov A. and Lugmair G. W. (2006) The Mn-Cr isotope systematics in the ureilites Kenna and LEW 85440. In *37th Lunar Planet. Sci. Conf., #1478 (abstr.)*.

Spicuzza M. J., Day J. M. D., Taylor L. A. and Valley J. W. (2007) Oxygen isotope constraints on the origin and differentiation of the Moon. *Earth Planet. Sci. Lett.* **253**, 254–265.

Spivak-Birndorf L., Wadhwa M., and Janney P. (2009) ^{26}Al-^{26}Mg systematics in D'Orbigny and Sahara 99555 angrites: Implications for high-resolution chronology using extinct chronometers. *Geochim. Cosmochim. Acta* **73**, 5202-5211.

Srinivasan P., McCubbin F. M., Agee C. B., Ziegler K., Sanborn M. E. and Yin Q.-Z. (2015) Petrologic and isotopic classifications of ungrouped achondrite NWA 8186: Implications for a CK/CV asteroidal origin. In *45th Lunar Planet. Sci. Conf., #1472 (abstr.)*.

Stöffler D., Keil K. and Scott E. R. D. 1991. Shock metamorphism of ordinary chondrites. *Geochim. Cosmochim. Acta* **55**, 3845-3867.

Sutton S. R., Wirick S. and Goodrich C. A. (2016) Ungrouped achondrite NWA 7325: titanium, vanadium and chromium XANES of mafic silicates record highly-reduced origin. *Meteorit. Planet. Sci*. submitted in revised form.

Takeda H. (1989) Mineralogy of coexisting pyroxenes in magnesian ureilites and their formation conditions. *Earth Planet. Sci. Lett.* **93**, 181-194.

Takeda H., Mori H. and Ogata H. (1989) Mineralogy of augite-bearing ureilites and the origin of their chemical trends. *Meteoritics* **24**, 73-81.

Takeda H., Mori H., Hiroi T. and Saito J. (1994) Mineralogy of new Antarctic achondrites with affinity to Lodran and a model of their evolution in an asteroid. *Meteoritics* **29**, 830-842.

Tenner T. J., Ushikubo T., Kurahashi E., Nagahara H. and Kita N. T. (2013) Oxygen isotope systematics of chondrule phenocrysts from the CO3.0 chondrite Yamato 81020: Evidence for two distinct oxygen isotope reservoirs *Geochim. Cosmochim. Acta* **102**, 226-245.

Tenner T. J. Nakashima D., Ushikubo T., Kita N. T. and Weisberg M. K. (2015) Oxygen isotope ratios of FeO-poor chondrules in CR3 chondrites: Influence of dust enrichment and H_2O during chondrule formation. *Geochim. Cosmochim. Acta* **148**, 228-250.

Trinquier A., Birck J-.L. and Allegre C. (2007) Widespread ^{54}Cr heterogeneity in the inner solar system. *Astrophysical Journal* **655**, 1179-1185.

Trinquier A., Elliott T., Ulfbeck D., Coath C., Krot A. N. and Bizzarro M. (2009) Origin of nucleosynthetic isotope heterogeneity in the solar protoplanetary disk. *Science* **324**, 374-376.

Ueda T., Yamashita K. and Kita N. (2006) Chromium isotopic study of ureilites. In *69th Annual Meeting of the Meoritical Society*, #5178 (abstr.).

Ushikubo T., Kimura M., Kita N. T. and Valley J. W. (2012) Primordial oxygen isotope reservoirs of the solar nebula recorded in chondrules in Acfer 094 carbonaceous chondrite. *Geochim. Cosmochim. Acta* **90**, 242-264.

Valley J. W., Spicuzza M. J. and Ushikubo T. (2014). Correlated $\delta^{18}O$ and [Ti] in lunar zircons: a terrestrial perspective for magma temperatures and water content on the Moon. *Contrib. Mineral. Petrol.* **167**, 956.

Wager L. R. and Brown G. M. 1967. Layered Igneous Rocks. Oliver and Boyd (Edinburgh and London).

Warren P. H. (2011a) Stable isotopes and the noncarbonaceous derivation of ureilites, in common with nearly all differentiated planetary materials. *Geochim. Cosmochim. Acta* **75**, 6912-6926.

Warren P.H. (2011b) Stable-isotopic anomalies and the accretionary assemblage of the Earth and Mars: A subordinate role for carbonaceous chondrites. *Earth Planet. Sci. Lett.* **311**, 93-100.

Warren P. H. and Kallemeyn G. W. (1989) Allan Hills 84025: the second brachinite, far more differentiated than Brachina, and an ultramafic achondritic clast from L chondrite Yamato 75097. Proceedings of the 19th Lunar and Planetary Science Conference. pp. 475-486.

Warren P. H. and Rubin A. E. (2010) Pyroxene-selective impact smelting in ureilites. *Geochim. Cosmochim. Acta* **74**, 5109-5133.

Warren P. H., Rubin A. E., Isa J., Brittenham S., Ahn I. and Choi B-G. (2013) Northwest Africa 6693: A new type of FeO-rich, low $\Delta^{17}O$, poikilitic cumulate achondrite. *Geochim. Cosmochim. Acta* **107**, 135-154.

Weber I., Bischoff A. and Weber D. (2003) TEM investigations on the monomict ureilites Jalanash and Hammadah al Hamra 064. *Meteorit. Planet. Sci.* **38**, 145-156.

Weber I., Morlok A., Bischoff A., Hiesinger H., Ward D. Joy K. H., Crowther S. A., Jastrzebski N. D., Gilmour J. D., Clay P. L., Wogelius R. A., Greenwood R. C., Franchi I. A. and Münker C. (2016) Cosmochemical and spectroscopic properties of Northwest Africa 7325 – A consortium study. *Meteorit. Planet. Sci.* **51**, 3-30.

Weider S. Z., Nittler L. R., Starr R. D., McCoy T. J., Stockstill-Cahill K. R., Byrne P. K., Denevi B. W., Head J. W. and Solomon S. C. (2012) Chemical heterogeneity on Mercury's surface revealed by the MESSENGER X-ray Spectrometer. *Journ. Geophys. Res.* **117**: E00L05, doi:10.1029/2012JE004153.

Williams C. D., Sanborn M. E. and Yin Q.-Z. (2016) Tracing petrogenetic links among planetary materials with Ti-Cr-O systematics. In 47th *Lunar Planet. Sci. Conf.*, *#1538 (abstr.)*.

Wilson L. W., Goodrich C. A. and Van Orman J. A. (2008) Thermal evolution and physics of melt extraction on the ureilite parent body. *Geochim. Cosmochim. Acta* **72**, 6154-6176.

Yamakawa A., Yamashita K., Makishima A. and Nakamura E. (2009) Chemical separation and mass spectrometry of Cr, Fe, Ni, Zn, and Cu in terrestrial and extraterrestrial materials using thermal ionization mass spectrometry. *Analytical Chemistry* **81**, 9787-9794.

Young E. D. and Russell S. S. (1998) Oxygen reservoirs in the early solar nebula inferred from an Allende CAI. *Science* **282**:452-455.

Young E. D., Ash R. D., England P. and Rumble D. III (1999) Fluid flow in chondritic parent bodies: deciphering the compositions of planetesimals. *Science* **286**,1331-1335.

Zhang J., Dauphas N., Davis. A. M. and Pourmand A. (2011) A new method for MC-ICPMS measurement of titanium isotopic composition: Identification of correlated isotope anomalies in meteorites. *Journal of Analytical Atomic Spectrometry* **26**, 2197-2205.

Table 1. Compositions of silicates in NWA 7325.

	Olivine (n=64)		Large pyroxenes (n=92)		Plagioclase (n=166)			
	Avg.	*SD*	*Avg.*	*SD*	*Avg.*	*SD*	*high An*	*low An*
SiO_2	40.5	*0.5*	53.0	*0.4*	45.1	*0.8*	46.9	45.0
TiO_2	na		bdl	*0.01*	bdl		bdl	bdl
Al_2O_3	0.05	*0.01*	2.79	*0.14*	34.4	*0.5*	33.5	34.6
Cr_2O_3	0.35	*0.02*	0.92	*0.07*	bdl		bdl	bdl
FeO	2.50	*0.15*	0.65	*0.05*	0.03	*0.02*	bdl	0.04
MgO	55.7	*0.1*	19.5	*0.1*	0.26	*0.07*	0.28	0.31
MnO	0.09	*0.01*	0.05	*0.02*	bdl		bdl	bdl
CaO	0.33	*0.02*	22.9	*0.1*	18.5	*0.3*	17.7	18.7
Na_2O	na		0.17	*0.02*	1.17	*0.13*	1.67	0.99
K_2O	na		na		bdl		bdl	bdl
SO_2	na		na		bdl		bdl	bdl
Total	99.6		100.0		99.5		100.2	99.7
Mg#	97.5	*0.1*	98.2	*0.2*				
Wo			45.3	*0.2*				
An					89.7	*1.1*	85.4	91.2
Or					0.0		0.0	0.0
Ab					10.3	*1.0*	14.6	8.8

Table 2. Endmember minerals used in spectral unmixing.

Quartz BUR-4120	Silica glass
Microcline BUR-3460	Quenched basalt
Albite WAR-0244	Fo0Fa100 [a]
Oligoclase BUR-060D	Fo10Fa90 [a]
Andesine BUR-240	Fo20Fa80 [a]
Labradorite WAR-4524	Fo30Fa70 [a]
Bytownite WAR-1384	Fo40Fa60 [a]
Anorthite BUR-340	Fo50Fa50 [a]
Actinolite HS-116.4B	Fo55Fa45 [a]
Biotite BIR-840	Fo65Fa35 [a]
Muscovite WAR-5474	Fo70Fa30 [a]
Chlorite WAR-1924	Fo75Fa25 [a]
Enstatite HS-9.4B	Fo80Fa20 [a]
Augite NMNH-9780	Fo89.5Fa10.5 [a]
Augite NMNH-122302	Fo100Fa0"
Serpentine HS-8.4B	Orthoclase WAR-RGSAN01
Serpentine BUR-1690	Oligoclase WAR-5804
Hematite BUR-2600	Pigeonite
Anhydrite ML-S9	Diopside WAR-5780
Gypsum ML-S6	Antigorite NMNH-47108
Calcite ML-C27	Ca-montmorillonite STx-1 solid
Dolomite ML-C28	Magnesiohastingsite HS-115.4B
Nontronite WAR-5108 granular	Magnesiohornblende WAR-0354
Fe-smectite SWa-1 solid	Hypersthene NMNH-B18247
Illite IMt-2 granular	Pyrite ML-SD
K-rich glass	Troilite ML-I9

[a] Synthetic olivine spectra from *Lane et al.,* 2011; otherwise spectra are from the Arizona State University spectral library (Christensen et al., 2000) or co-author Lane's collection.

Table 3. Oxygen isotope ratios of minerals in NWA 7325.

Mineral (mode %)	$\delta^{18}O$ ‰	$\delta^{17}O$ ‰	$\Delta^{17}O$ ‰
Olivine (13%), n=7	7.6 ±0.3	3.0 ±0.2	–0.97 ±0.17
Pyroxene (28%), n=7	7.3 ±0.2	3.0 ±0.2	–0.84 ±0.17
Plagioclase (58%), n=4	7.9 ±0.4	3.2 ±0.3	–0.90 ±0.20
Average*	7.7 ±0.4	3.1 ±0.3	–0.90 ±0.13

Errors quoted are 95% confidence level.
*Average values of $\delta^{18}O$ and $\delta^{17}O$ are weighted by modal volume % and the average of $\Delta^{17}O$ value is from the mean of 18 spot analyses.

Table 4. Trace element concentrations (ppm) of plagioclase in NWA 7325.

Elements	Mg	K	Sc	Ti	Cr	Mn	Fe	Rb	Sr	Ba
Mean (n=7)	1420	26	0.3	12	6	9	180	0.09	320	0.22
SD %	15	16	52	27	59	37	36	69	0.6	32

Table 5. Chromium and titanium isotopic compositions of NWA 7325 and Acapulco.

Sample	ε^{54}Cr (±2SE)	ε^{46}Ti (±2SE)	ε^{48}Ti (±2SE)	ε^{50}Ti (±2SE)
NWA 7325	-0.61±0.11	-0.42±0.13	-0.06±0.08	-1.58±0.33
Acapulco	-0.70±0.10	-0.40±0.13	-0.03±0.09	-1.48±0.45

Table 6. Trace element abundances in parent melt of NWA 7325 estimated from plagioclase trace element compositions.

	MgO (%)	K (ppm)	Ti (ppm)	Sr (ppm)	Ba (ppm)
Plagioclase	0.23	26	12	320	0.22
D(plagioclase/melt)[*1]	0.037	0.16	0.036	0.92	0.084
Parent melt	6.3	170	320	350	2.6
Abundance/CI[*2]		0.30	0.73	45	1.1

[*1] Values for Mg, K, Sr and Ba are from Dohmen and Blundy (2014) assuming Na_2O and CaO wt% of parent melt to be the same as those of bulk 7325 (Barrat et al., 2015). Value for Ti is from Bindemann et al. (1998), assuming T=1500 K and plagioclase composition (X_{An}=0.9).
[*2]CI chondrite abundance is from Anders and Grevesse (1989).

Table 7. Percent mixing (min-max range) of chondrite end-member required to generate NWA 7325 composition from ureilite.

	$\varepsilon^{54}Cr$-$\Delta^{17}O$		$\varepsilon^{50}Ti$- $\Delta^{17}O$		$\varepsilon^{50}Ti$- $\varepsilon^{54}Cr$	
Chondrite Group	*Min (%)*	*Max (%)*	*Min (%)*	*Max (%)*	*Min (%)*	*Max (%)*
CI	10	39	0	49	4	34
CM	11	33	0	29	4	36
CO	13	20	0	20	6	24
CV	11	24	0	22	4	20
CR	8	20	-	-	-	-
H	31	52	0	52	14	86
L	21	49	0	47	14	84
LL	26	45	0	44	16	88
EH	20	65	0	72	10	66
EL	15	68	-	-	-	-

Figure Captions

Fig. 1. Collage of back-scattered electron images (BEI) of studied thick section of NWA 7325. The rock has a protogranular to poikilitic texture of 25-30% high-Ca pyroxene (pyx) and 10-15% olivine (ol) grains, surrounded or poikilitically enclosed by 55-60% plagioclase (plag).

Fig. 2. BEI of NWA 7325. (a) Olivine (ol) grains are rounded with concave segments, and commonly occur as partial or complete mantles around pyroxenes (pyx). (b) Plagioclase has a mottled appearance and shows reacted boundaries with both olivine and pyroxene grains. (c) Pyroxene grains in contact with plagioclase show resorbed edges, with idiomorphic reentrants into plagioclase. (d) Plagioclase in contact with olivine grains contains numerous tiny inclusions of Ca-rich pyroxene, often with elongated shapes and parallel alignment, while olivine grains have smooth edges. (e) Grain of troilite showing fine lamellae of Cr-rich phase inferred to be daubreelite. (f) Grain of troilite at pyroxene-olivine-plagioclase junction. Plagioclase shows reaction with both sulfide and pyroxene, but not with olivine.

Fig. 3. Compositions of olivine in NWA 7325 compared with olivine in various asteroidal achondrites and rare magnesian anorthitic (Mg-An) clasts in polymict ureilites. (a) Molar Fe/Mg vs. Fe/Mn. (b) Wt.% CaO vs. wt.% Cr_2O_3. The composition of NWA 7325 olivine is not like that of any known achondrites, but is close to compositions of magnesian anorthitic clasts in polymict ureilites. Data for brachinites and brachinite-like achondrites from Nehru et al. (1983), Warren and Kallemeyn (1989), Goodrich and Righter (2000), Mittlefehldt et al. (2003), Goodrich et al. (2006, 2011, 2015), Day et al. (2012), Gardner-Vandy et al. (2013) and Meteoritical Bulletin Database. Data for ungrouped achondrites Zag(b) from Delaney et al. (2000), Divnoe from Petaev et al. (1994), Tafassasset from Gardner-Vandy et al. (2012), LEW 88763 from Gardner-Vandy (2012) and Day et al (2015), and GRA 06128/06129 from Shearer et al. (2010) and Day et al. (2012). For sources of ureilite, lodranite, and winonaite data, see Fig. 5 of Goodrich et al. (2011). Data for pallasites from Mittlefehldt et al. (1998). Data for magnesian anorthitic clasts in polymict ureilites from Ikeda et al. (2000), Kita et al. (2004), Cohen et al. (2004) and Goodrich and Wilson (2014).

Fig. 4. Mg# vs. wt.% Al_2O_3 for high-Ca pyroxene in NWA 7325 compared with various asteroidal achondrites and magnesian anorthitic clasts in polymict ureilites. The composition of NWA 7325 pyroxene is unique on this plot compared with known achondrites, but similar to that in magnesian anorthitic clasts in polymict ureilites. Data for ureilites from Takeda (1989), Takeda et al. (1989), Goodrich et al. (2009, 2014 and references therein), and Weber et al. (2003). Data for brachinites and brachinite-like achondrites from Nehru et al. (1983), Warren and Kallemeyn (1989), Mittlefehldt et al. (2003), Goodrich et al. (2011) and Gardner-Vandy et al. (2013). Data for ungrouped achondrites Zag(b) from Delaney et al. (2000), Divnoe from Petaev et al. (1994), Tafassasset from Gardner-Vandy et al. (2012), LEW 88763 from Gardner-Vandy (2012) and Day et al. (2015), and GRA 06128/06129 from Shearer et al. (2010) and Day et al. (2012). Data for angrites from Mittlefehldt et al. (1998). Data for acapulcoites and lodranites from Takeda et al. (1994), Mittlefehldt et al. (1996) and Burroni and Folco (2008). Data for winonaites from Kimura et al. (1992). Data for magnesian anorthitic clasts in polymict ureilites from Ikeda et al. (2000), Kita et al. (2004), Cohen et al. (2004), Goodrich and Wilson (2014), and this work.

Fig. 5. Plot of An# in plagioclase vs. Mg# of olivine and/or pyroxene in NWA 7325 compared with various asteroidal achondrites and feldspathic clasts in polymict ureilites. The combination of very An-rich plagioclase and very magnesian mafic minerals in NWA 7325 is unique compared with any known asteroidal achondrites, but very similar to that of the magnesian anorthitic population of feldspathic clasts in polymict ureilites. ac/lod = acapulcoites and lodranites; brach = brachinites and brachinite-like achondrites. Sources of data as in figures 3 and 4.

Fig. 6. (a) BEI showing vein of plagioclase with idiomorphic side protrusions in pyroxene in NWA 7325. (b) BEI showing mottled appearance of plagioclase in NWA 7325. (c) Higher magnification image of plagioclase. Mottled appearance is caused by fine (≤2 μm wide) linear features, which consist of darker zones with central "rosettes" of a brighter phase. Box indicates area of x-ray maps in [d-f]. (d-f) Mg, Al and Si x-ray maps of area in box in [c], showing that darker areas have lower Al and higher Si than surrounding plagioclase, while bright rosettes have

higher Mg and Al and lower Si. Rosettes may be spinel, with the darker zones being Al-depleted (Na-enriched) plagioclase.

Fig. 7. Small grains of pyroxene showing reaction textures with surrounding plagioclase in NWA 7325. (a) BEI. Note that plagioclase immediately surrounding and protruding into the pyroxene grain is darker than the bulk of the plagioclase. (b) Na-Ca-Al x-ray map of the area in [a], showing that the reaction zone of plagioclase around the pyroxene grain is more sodic than the bulk of the plagioclase. (c) BEI. Pyroxene grain showing two distinct cores. Tiny crystals of very bright phase in partial halo around the pyroxene were tentatively identified as wollastonite. (d) Profiles of Ca, Mg, Al and Fe along profile 7 marked in [c]. Rims are enriched in Ca, and depleted in Mg, Al and Fe relative to the cores. Explanation for elevated Al between the two cores is unclear.

Fig. 8. Mid-infrared emissivity spectrum of NWA 7325 (blue). The spectrum is an average of nine individual spectra (which are each 256 co-added scans acquired during measurement). Also shown is modeled spectrum of NWA 7325 (orange) and the spectra of the identified mineral components (black). The emissivity spectrum of NWA 7325 is repeated at the bottom of the figure (blue) superposed by the reflectance data of Weber et al. (2016) converted to emissivity (green) for comparison.

Fig. 9. (a) Oxygen three-isotope analyses of NWA 7325 minerals using SIMS. Individual data points represent single SIMS analyses. Olivine, pyroxene, and anorthite are shown as squares, triangles and diamonds, respectively. One anorthite analysis shown as open symbol hit a vein in the plagioclase and the data deviate beyond analytical uncertainty. Laser fluorination analyses of bulk chips (Irving et al., 2013; Weber et al., 2016), mineral separates (plagioclase "Pl" and pyroxene "Px"; Jabeen et al. 2014), and a bulk powder (Barrat et al., 2015) are shown as open circles. The range of ureilite bulk analyses (Clayton and Mayeda, 1996) is enclosed by dotted line. Terrestrial fractionation (TF) and carbonaceous chondrite anhydrous mineral (CCAM) lines are shown for reference. (b) Oxygen isotope ratios of bulk achondrites (Clayton and Mayeda, 1996; Yamaguchi et al., 2002; Greenwood et al. ,2012) and Mg-An-rich clasts in DaG 319 polymict ureilite (Kita et al. 2004) are compared to the average value of three minerals in NWA

7325 (Table 4). Ranges of HED meteorites, Martian meteorites (Mars) and terrestrial mantle and lunar samples (Earth-Moon) are also shown as oval areas. The primitive chondrule mineral (PCM) line (Ushikubo et al., 2012) is shown along with the TFL and CCAM lines as references.

Fig. 10. Selected trace element concentrations in plagioclase in NWA 7325, polymict ureilites, and basaltic achondrites. NWA 7325 data points represent individual analysis spots (Online Supporting Information, Table S2), excluding 2 analyses that hit veins in plagioclase. Polymict ureilite data are from Kita et al. (2004). Filled diamonds are for magnesian anorthitic plagioclase clast in polymict ureilite DaG 319. Data for albitic and labradoritic lithology clasts in polymict ureilites shown as grey squares. Data from eucrites, angrites, and ungrouped achondrite NWA 011 are shown as the total range reported in Hsu and Crozaz (1996, 1997) and Floss et al. (2003, 2005).

Fig. 11. (a) Comparison of $\Delta^{17}O$ and $\varepsilon^{54}Cr$ isotopic composition of NWA 7325 with other achondrite and carbonaceous chondrite groups. Dashed lines represent examples of mixing curves between ureilite compositions (range indicated by green box) and various chondrite end-members that pass through the composition of NWA 7325. Mixing lines were calculated by adding 2% increments of the chondrite end-members to the ureilite composition. Literature data for $\Delta^{17}O$ are from Clayton and Mayeda (1996, 1999), Clayton et al. (1984, 1991), Scott et al. (2009), Jenniskens et al. (2012, 2014) and Popova et al. (2013). Literature data for $\varepsilon^{54}Cr$ are from Ueda et al. (2006), Shukolyukov and Lugmair (2006), Trinquier et al. (2007), Jenniskens et al. (2012, 2014) and Popova et al. (2013). (b) Comparison of $\Delta^{17}O$ and $\varepsilon^{50}Ti$ of NWA 7325 with other achondrite and carbonaceous chondrite groups. Literature data for $\Delta^{17}O$ same as figure (a) and literature data for $\varepsilon^{50}Ti$ are from Trinquier et al. (2009), Leya et al. (2008), and Zhang et al. (2011). (c) $\varepsilon^{54}Cr$ versus $\varepsilon^{50}Ti$ comparison plot of NWA 7325 and other meteorite groups. Each meteorite group is shown as a composite point averaging multiple samples within a group using the references given for (a) and (b). The values for NWA 7325 and Acapulco are given in Table 5.

Fig. 12. BEI of magnesian anorthitic clast (clast 9) in polymict ureilite NWA 10657_003. Clast consists of plagioclase of An 86-89 with an internal texture including small, dispersed pyroxene

grains, reacted "islands" of high-Ca pyroxene, and "veins" of Na-enriched plagioclase + Mg, Al-rich phase inferred to be spinel, similar to plagioclase in NWA 7325 (see figures 6 and 7). Areas outlined by boxes in [a] are shown at higher magnification in [b] and [c]. Linear features seen in plagioclase in [c] are shown at higher magnification in [d].

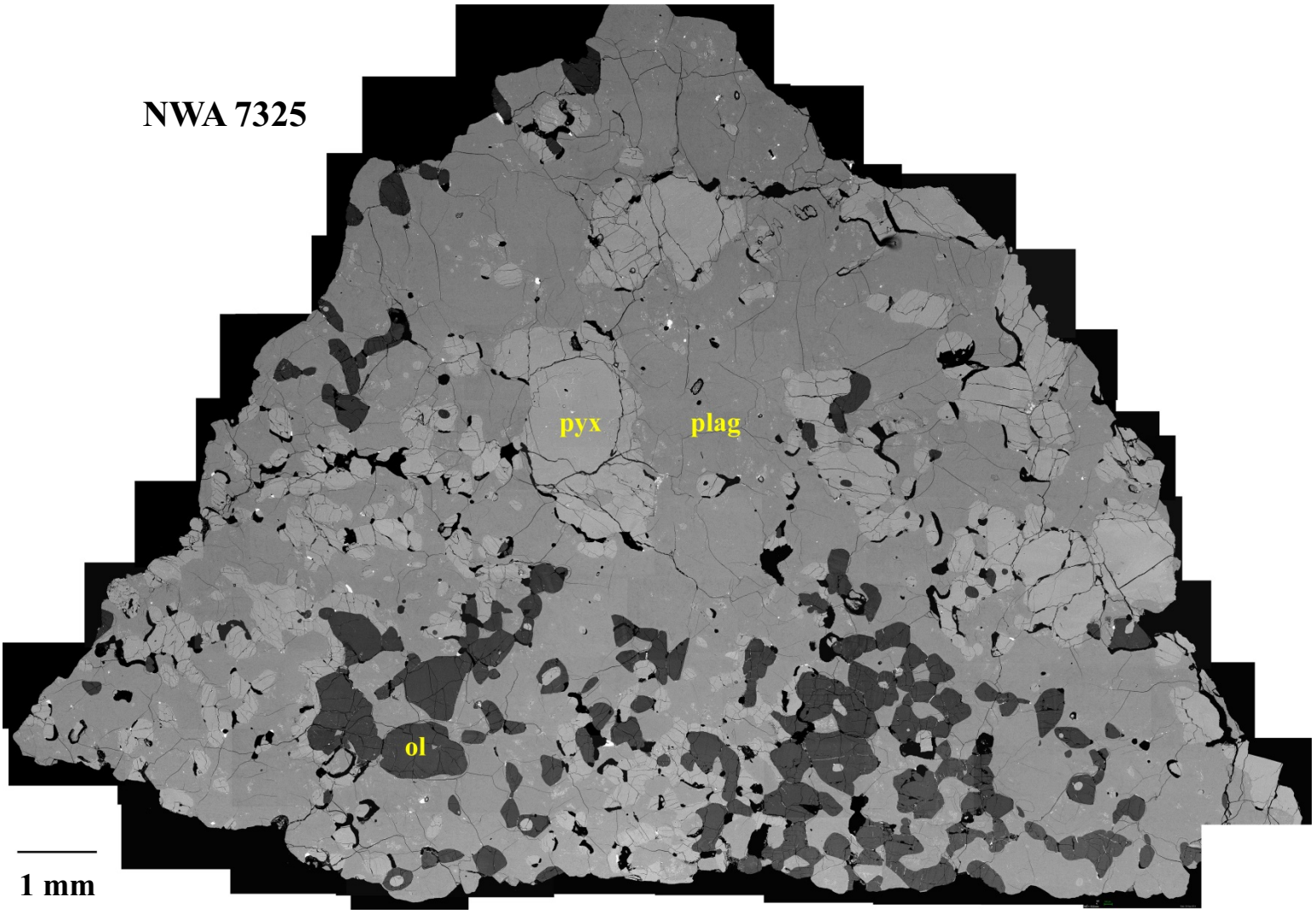

Fig. 1

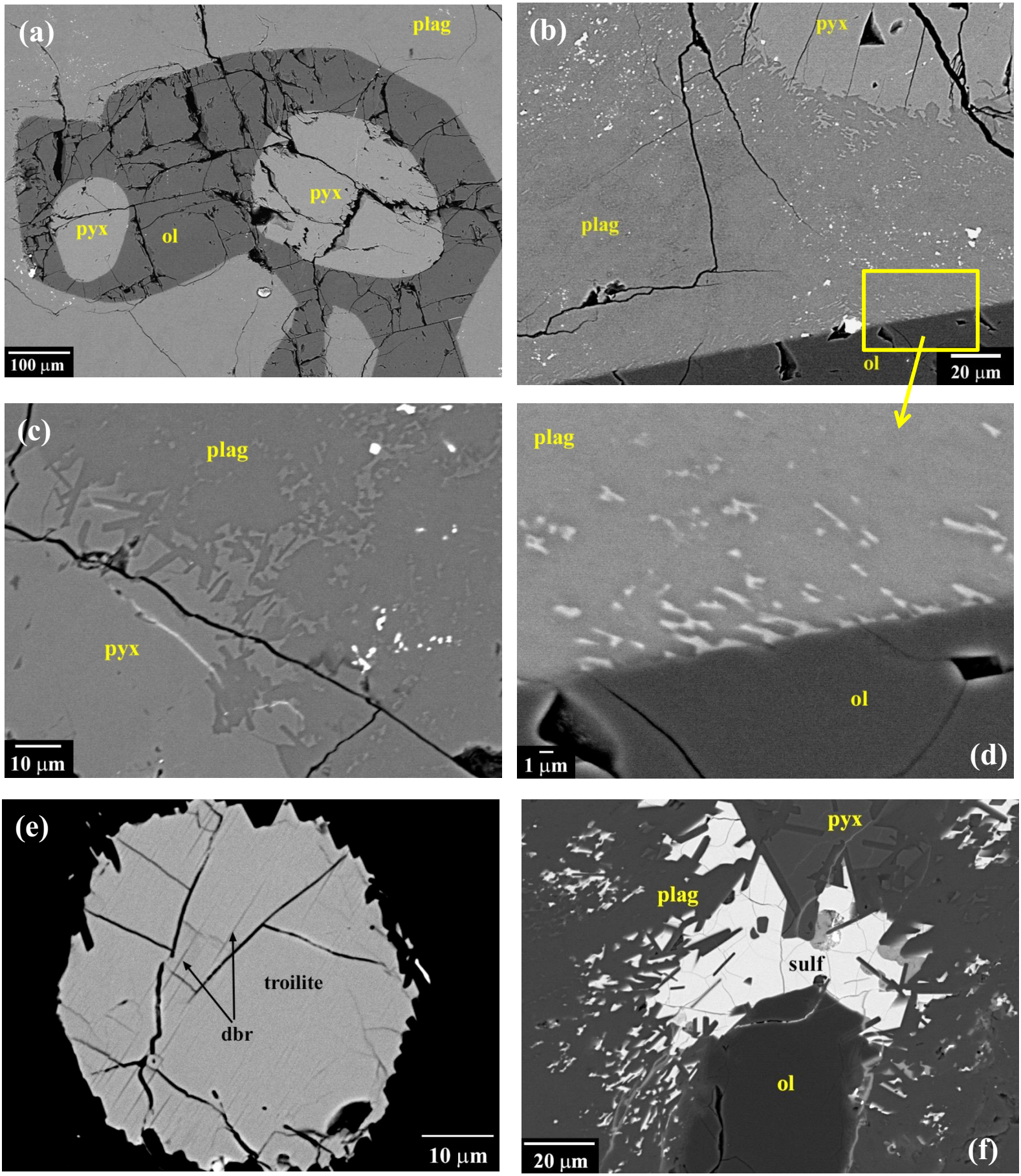
(a)
plag
pyx
pyx
ol
100 μm
(b)
pyx
plag
ol
20 μm
(c)
plag
pyx
10 μm
plag
ol
1 μm
(d)
(e)
troilite
dbr
10 μm
pyx
plag
sulf
ol
20 μm
(f)

Fig. 2

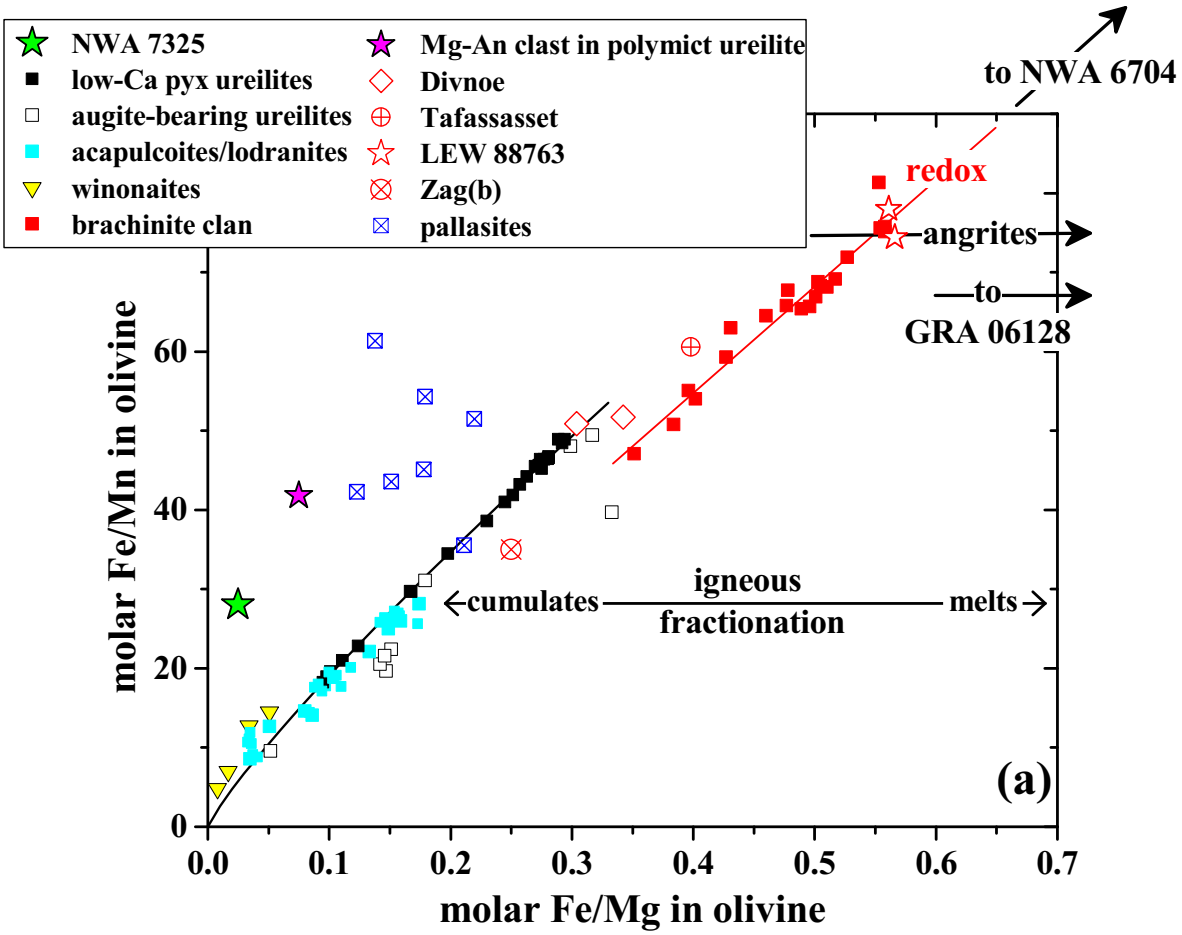
NWA 7325
low-Ca pyx ureilites
augite-bearing ureilites
acapulcoites/lodranites
winonaites
brachinite clan
Mg-An clast in polymict ureilite
Divnoe
Tafassasset
LEW 88763
Zag(b)
pallasites
to NWA 6704
redox
angrites
to
GRA 06128
cumulates
igneous
fractionation
melts
(a)
molar Fe/Mn in olivine
molar Fe/Mg in olivine
0
20
40
60
0.0
0.1
0.2
0.3
0.4
0.5
0.6
0.7

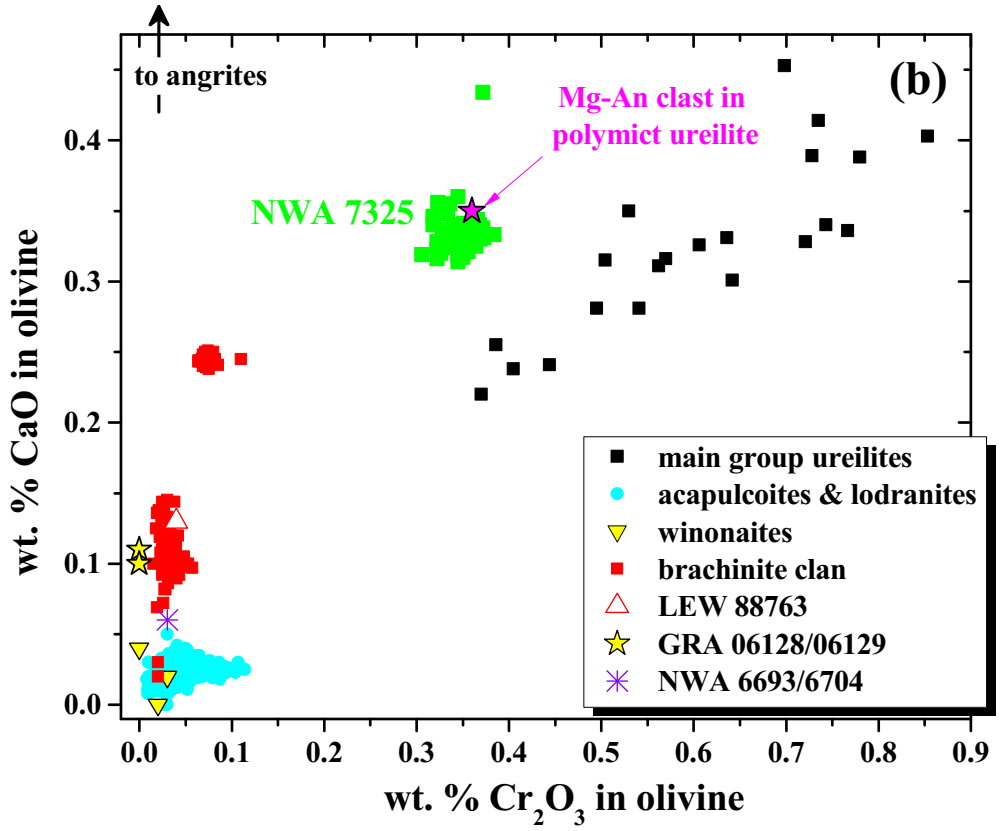
to angrites
(b)
Mg-An clast in
polymict ureilite
NWA 7325
main group ureilites
acapulcoites & lodranites
winonaites
brachinite clan
LEW 88763
GRA 06128/06129
NWA 6693/6704
wt. % CaO in olivine
wt. % Cr2O3 in olivine
0.0
0.1
0.2
0.3
0.4
0.5
0.6
0.7
0.8
0.9

Fig. 3

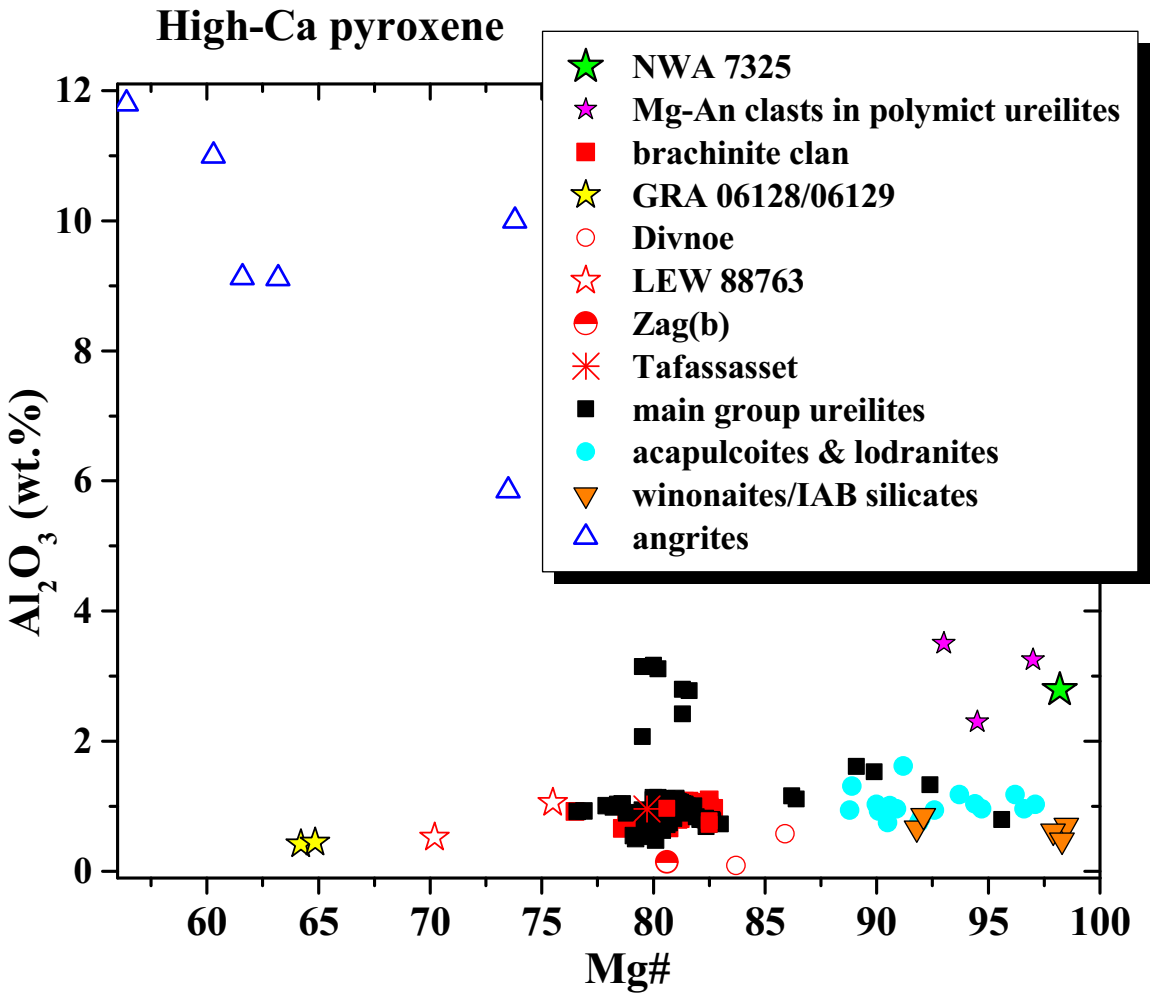
High-Ca pyroxene
NWA 7325
Mg-An clasts in polymict ureilites
brachinite clan
GRA 06128/06129
Divnoe
LEW 88763
Zag(b)
Tafassasset
main group ureilites
acapulcoites & lodranites
winonaites/IAB silicates
angrites
Al2O3 (wt.%)
Mg#
0
2
4
6
8
10
12
60
65
70
75
80
85
90
95
100

Fig. 4

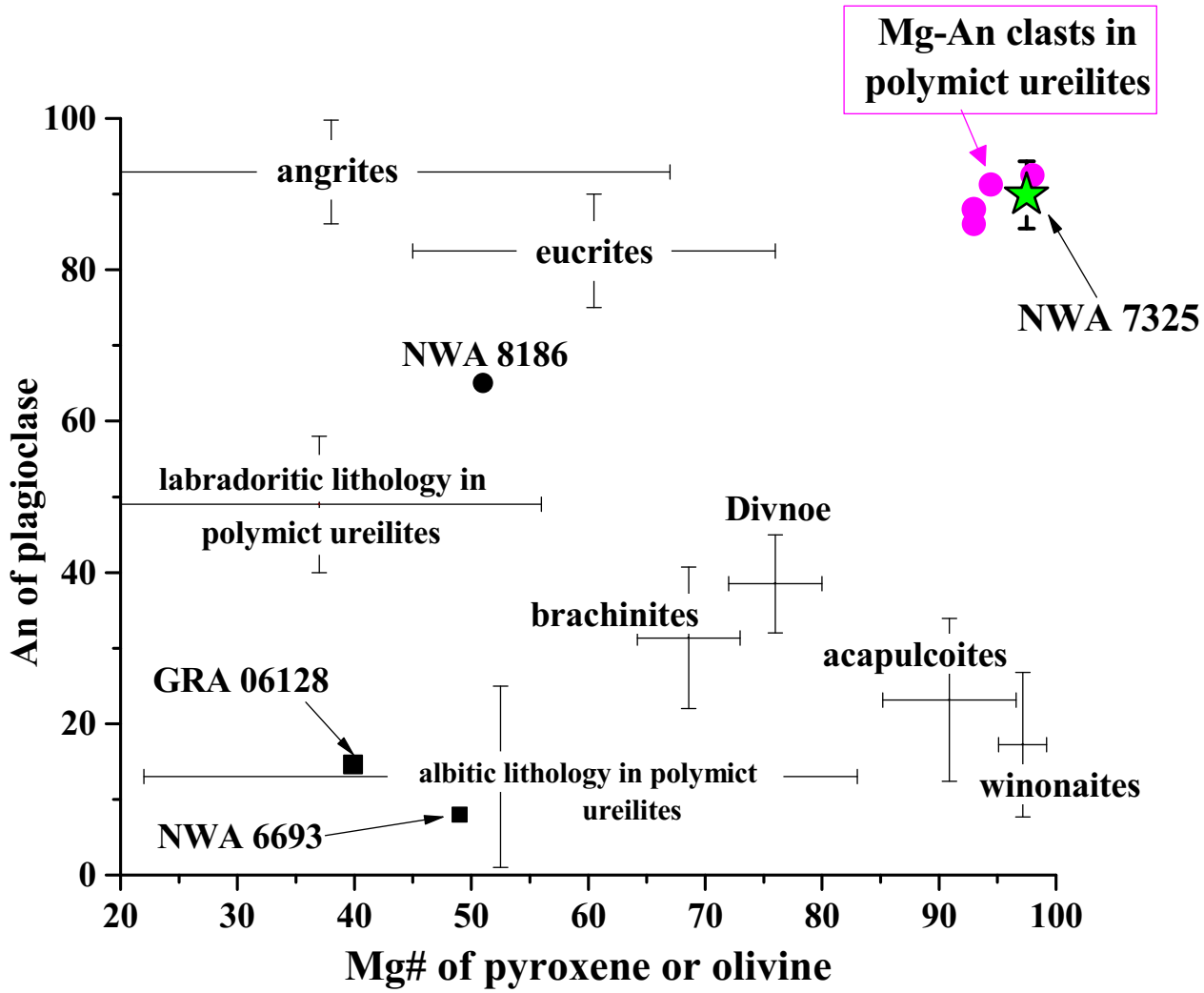
Mg-An clasts in polymict ureilites
NWA 7325
angrites
eucrites
NWA 8186
labradoritic lithology in polymict ureilites
Divnoe
brachinites
acapulcoites
winonaites
GRA 06128
albitic lithology in polymict ureilites
NWA 6693
An of plagioclase
Mg# of pyroxene or olivine
0
20
40
60
80
100
20
30
40
50
60
70
80
90
100

Fig. 5

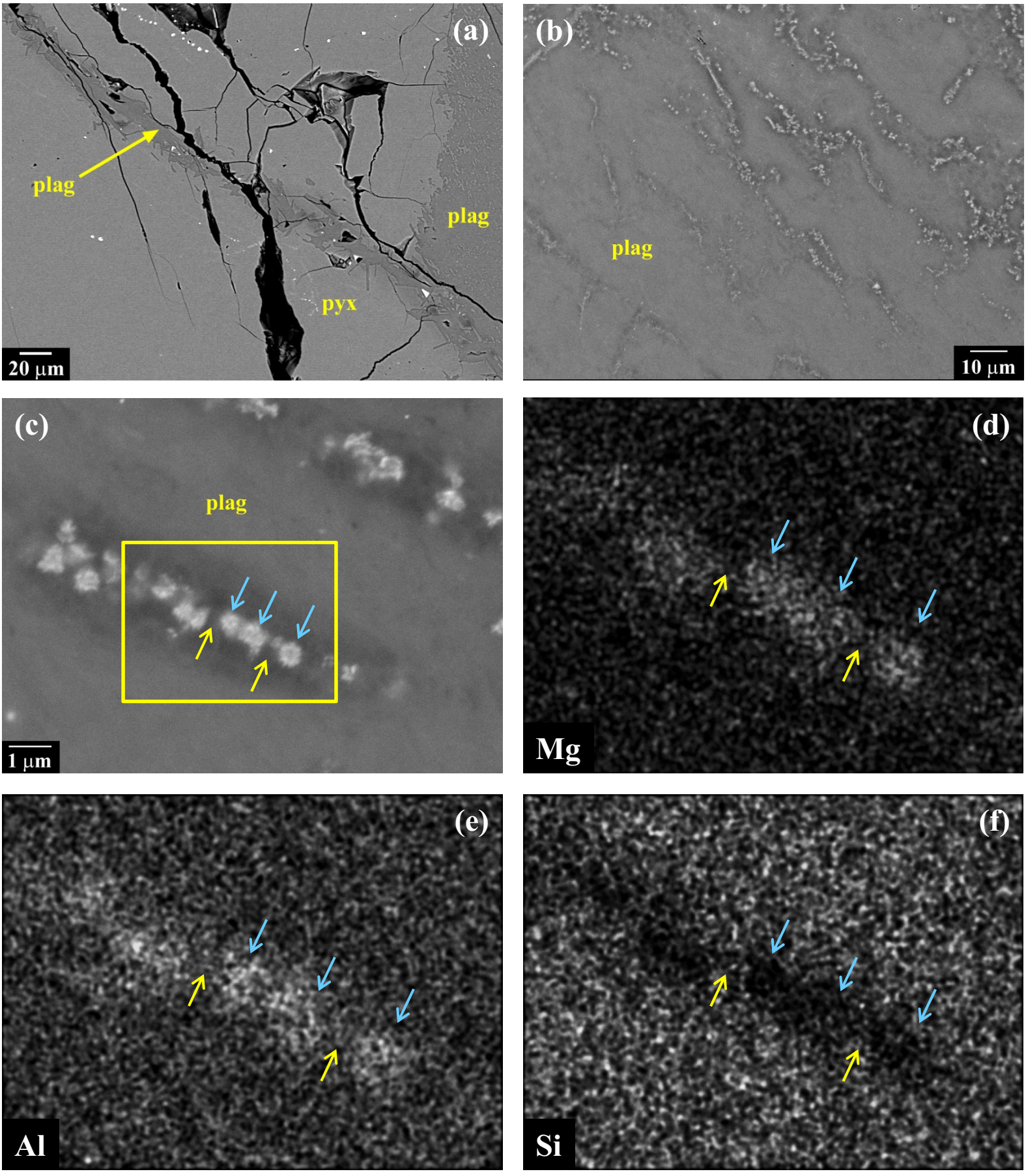

Fig. 6

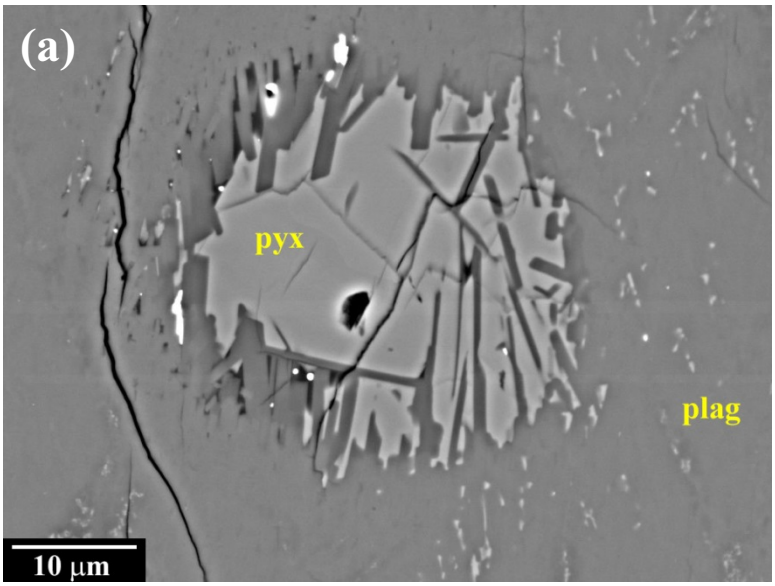
(a)
pyx
plag
10 μm

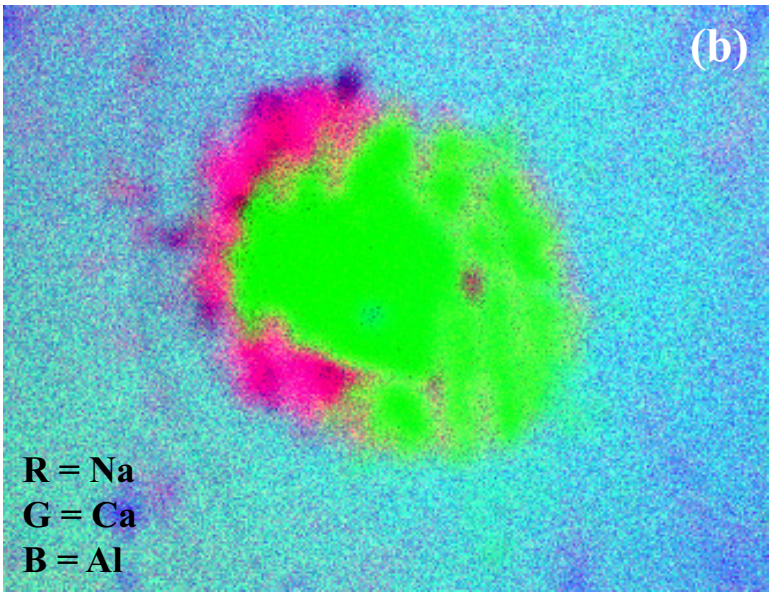
(b)
R = Na
G = Ca
B = Al

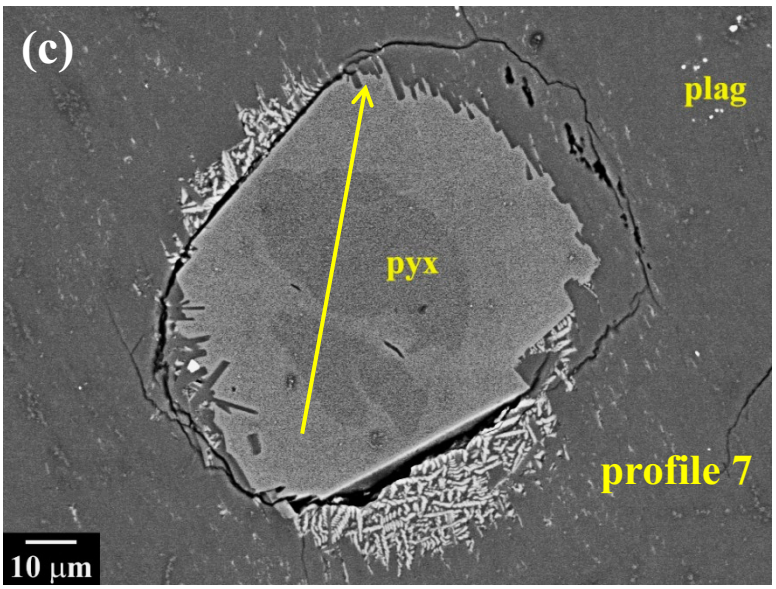
(c)
plag
pyx
profile 7
10 μm

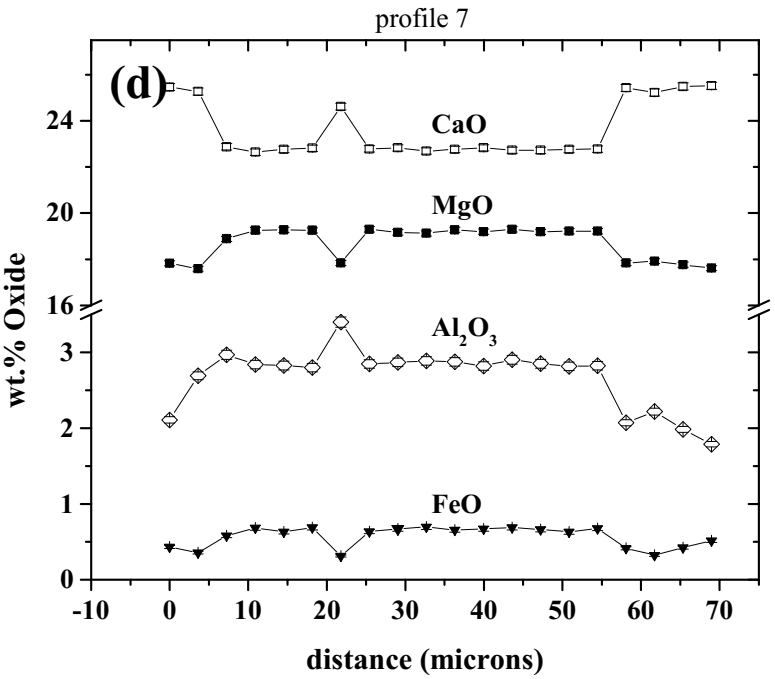
profile 7
(d)
CaO
MgO
Al2O3
FeO
wt.% Oxide
distance (microns)
24
20
16
3
2
1
0
-10
0
10
20
30
40
50
60
70

Fig. 7

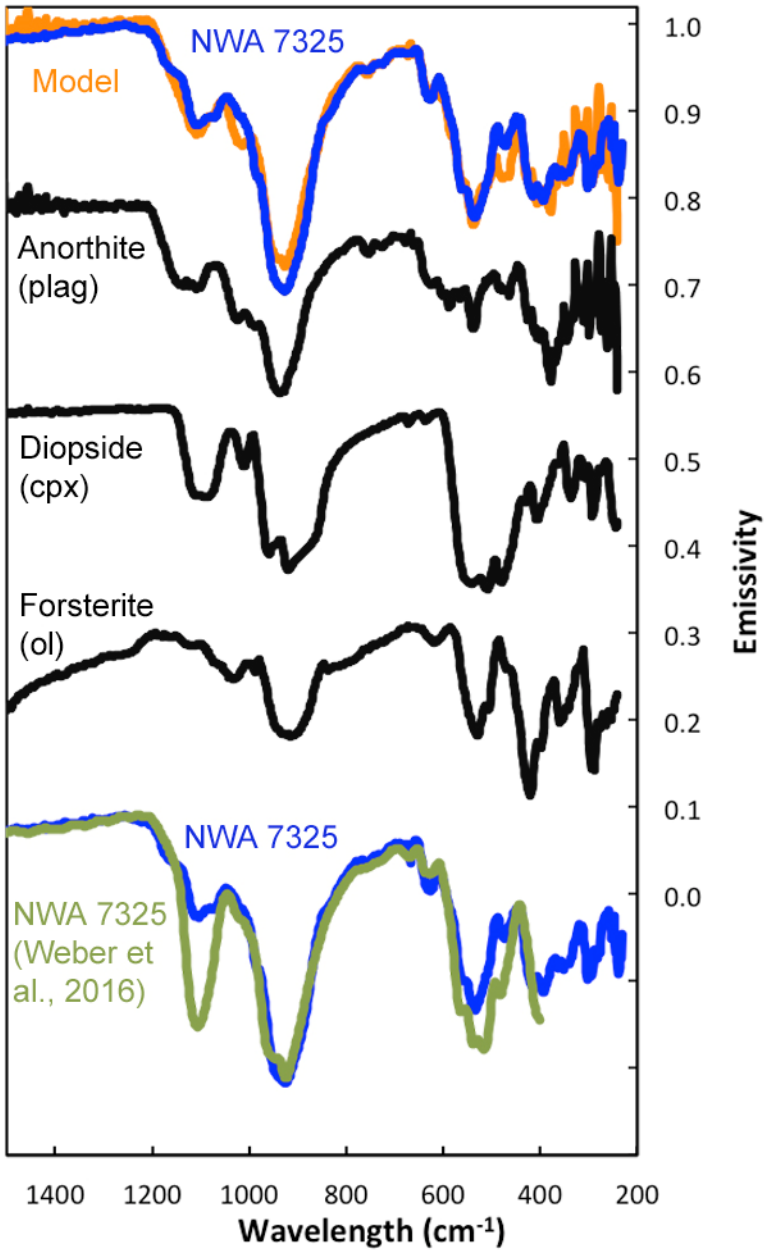
NWA 7325
Model
Anorthite
(plag)
Diopside
(cpx)
Forsterite
(ol)
NWA 7325
NWA 7325
(Weber et
al., 2016)
1.0
0.9
0.8
0.7
0.6
0.5
0.4
0.3
0.2
0.1
0.0
Emissivity
1400
1200
1000
800
600
400
200
Wavelength (cm-1)

Fig. 8

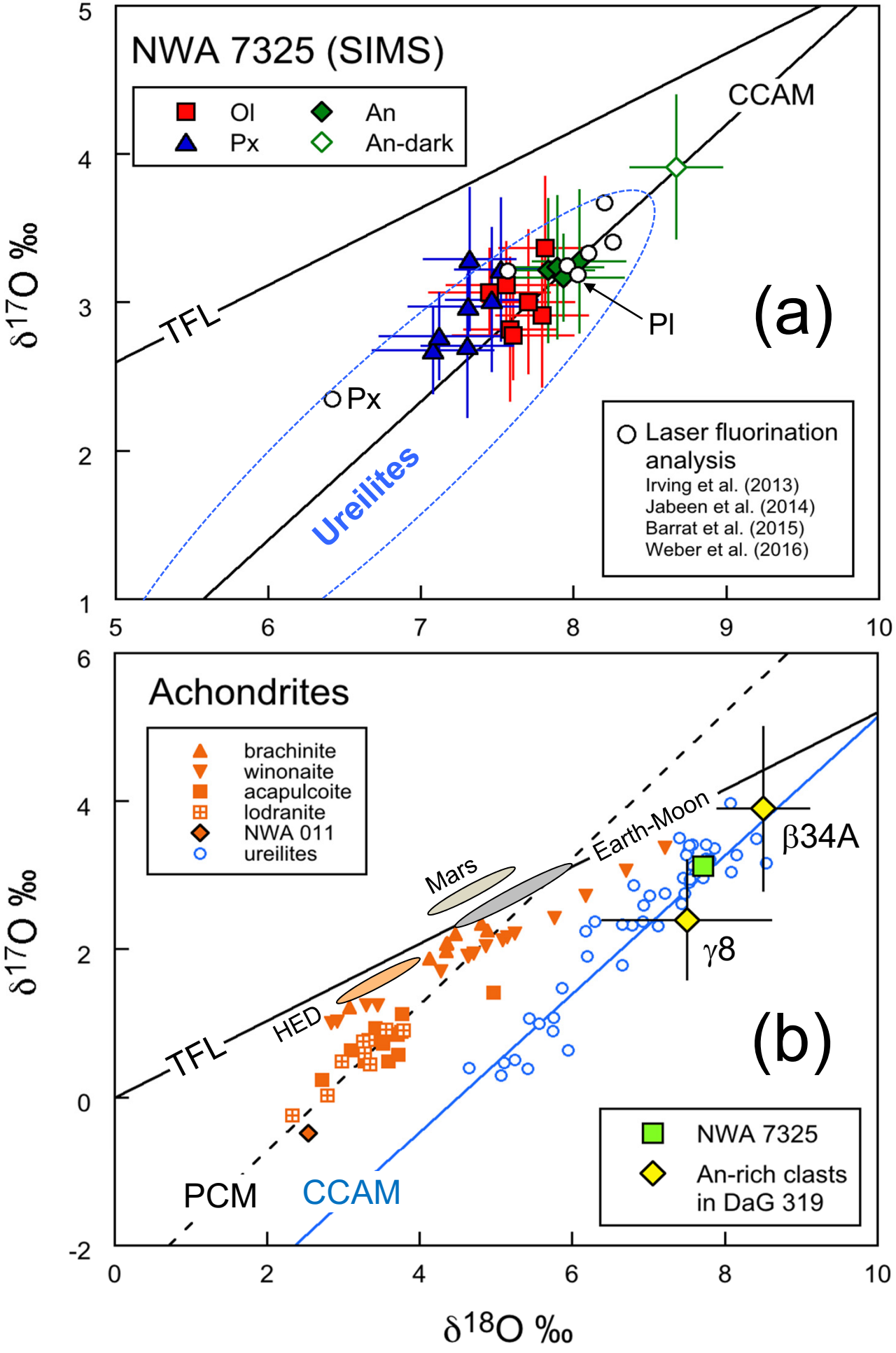
NWA 7325 (SIMS)
Ol
Px
An
An-dark
CCAM
TFL
Pl
(a)
Px
Ureilites
Laser fluorination analysis
Irving et al. (2013)
Jabeen et al. (2014)
Barrat et al. (2015)
Weber et al. (2016)
δ17O ‰
Achondrites
brachinite
winonaite
acapulcoite
lodranite
NWA 011
ureilites
Mars
Earth-Moon
β34A
γ8
HED
TFL
(b)
NWA 7325
An-rich clasts in DaG 319
PCM
CCAM
δ18O ‰

Fig. 9

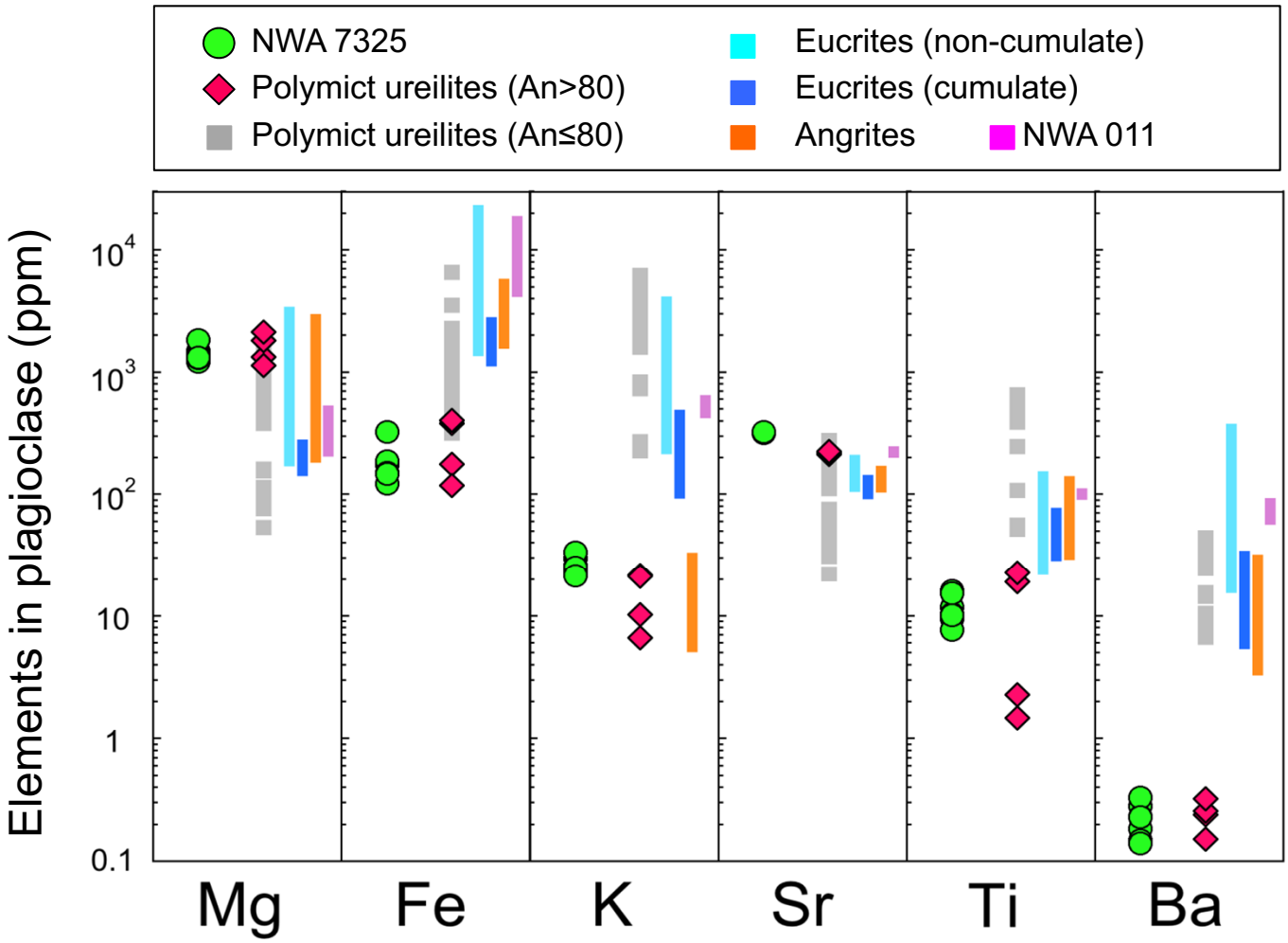
NWA 7325
Polymict ureilites (An>80)
Polymict ureilites (An≤80)
Eucrites (non-cumulate)
Eucrites (cumulate)
Angrites
NWA 011
Elements in plagioclase (ppm)
10^4
10^3
10^2
10
1
0.1
Mg
Fe
K
Sr
Ti
Ba

Fig. 10

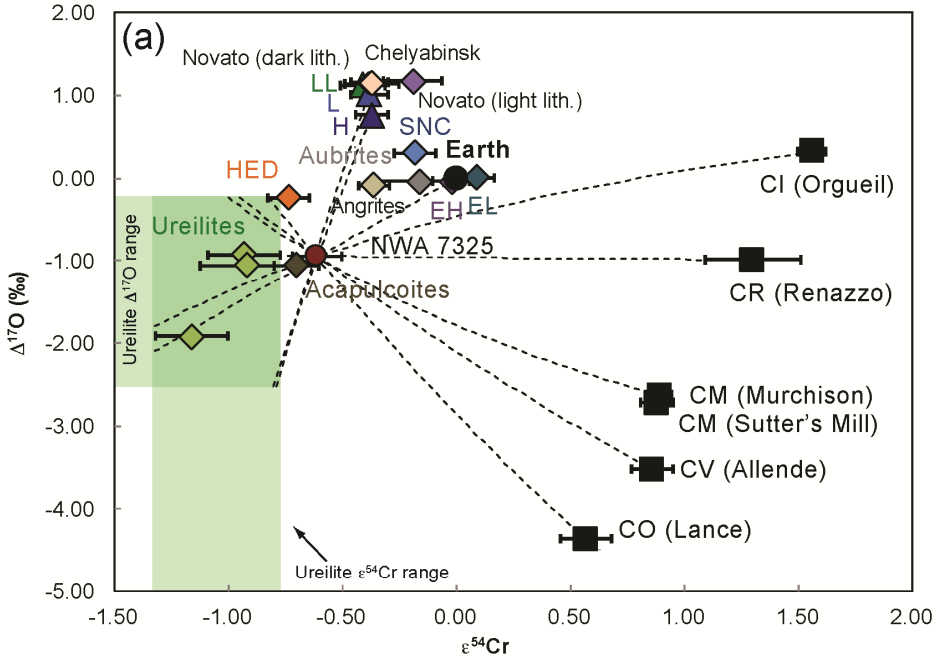
(a)
Novato (dark lith.)
Chelyabinsk
Novato (light lith.)
LL
L
H
SNC
Earth
Aubrites
HED
Angrites
EH
EL
Ureilites
NWA 7325
Acapulcoites
CI (Orgueil)
CR (Renazzo)
CM (Murchison)
CM (Sutter's Mill)
CV (Allende)
CO (Lance)
Ureilite Δ17O range
Ureilite ε54Cr range
Δ17O (‰)
ε54Cr

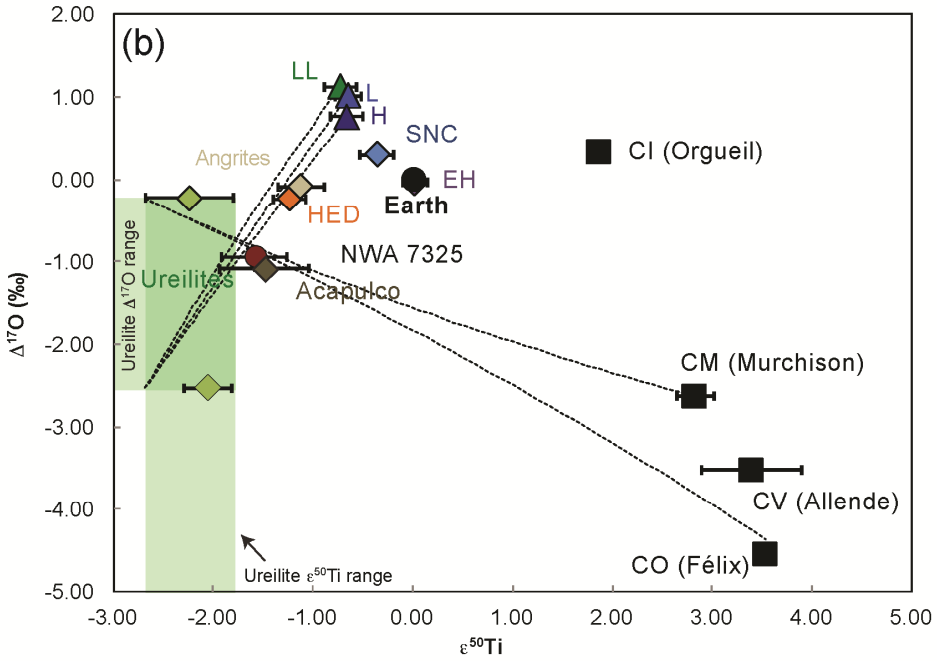
(b)
LL
L
H
SNC
EH
Earth
Angrites
HED
CI (Orgueil)
NWA 7325
Ureilites
Acapulco
CM (Murchison)
CV (Allende)
CO (Félix)
Ureilite Δ17O range
Ureilite ε50Ti range
Δ17O (‰)
ε50Ti

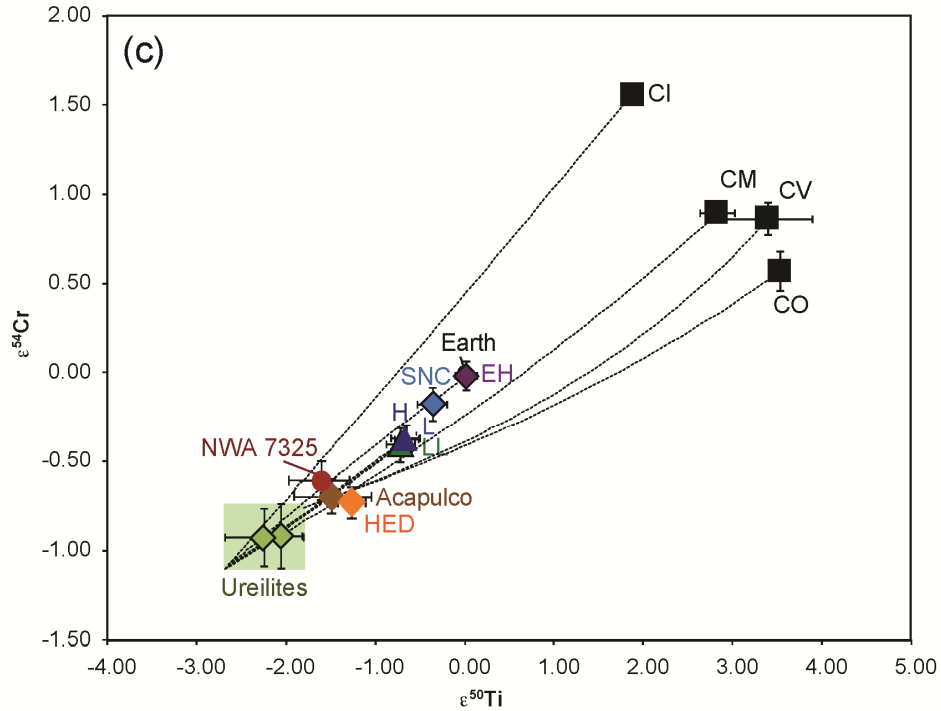
(c)
CI
CM
CV
CO
Earth
SNC
EH
H
L
LL
NWA 7325
Acapulco
HED
Ureilites
ε54Cr
ε50Ti

Fig. 11

Clast 9 in NWA 10657_003 polymict ureilite

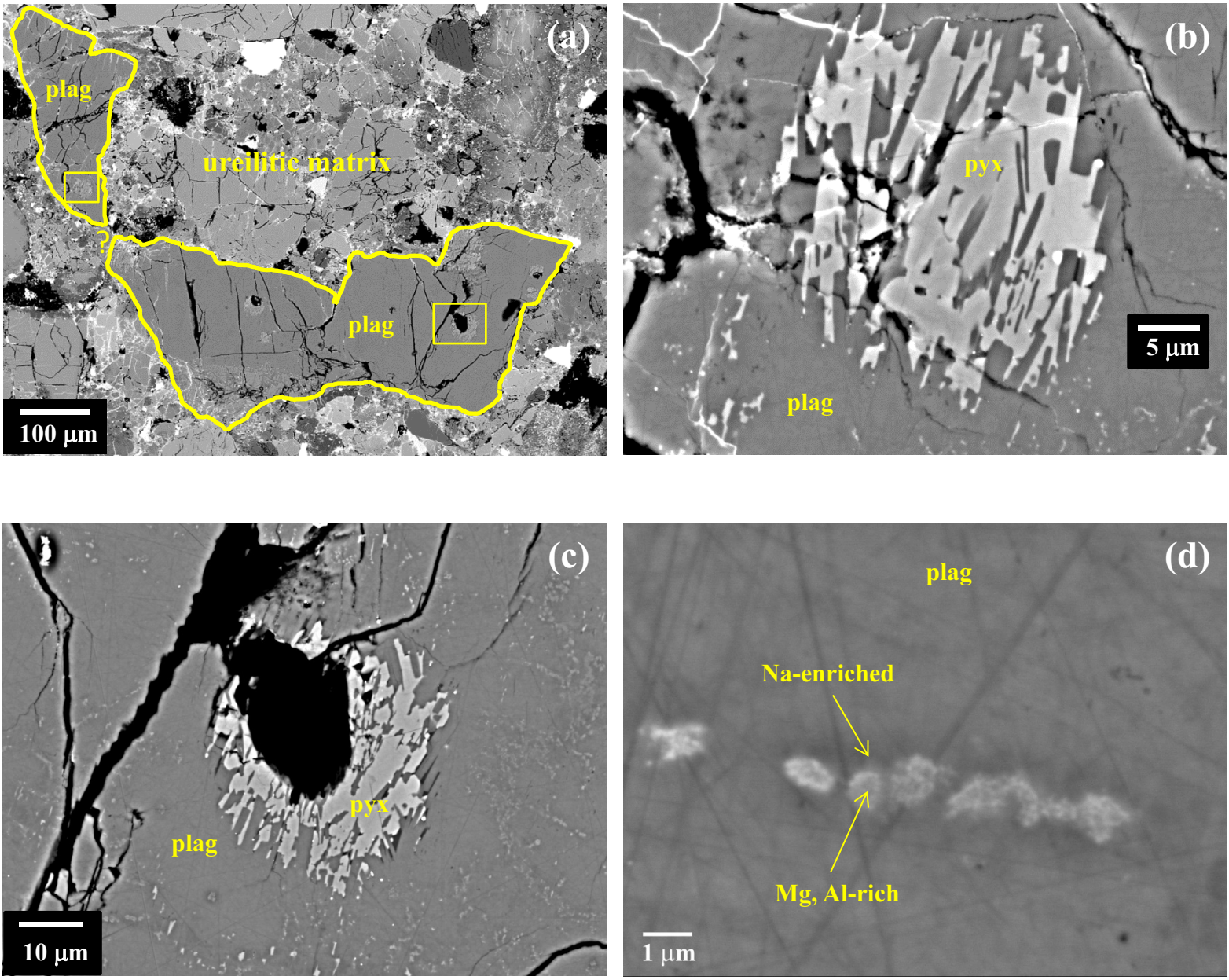

Fig. 12